The Thesis Committee for Gabrielle Marie Varona
Certifies that this is the approved version of the following Thesis:

Hydrate-bearing sands in the Terrebonne Basin record the transition from ponded deposition to bypass in the deep-water Gulf of Mexico

APPROVED BY
SUPERVISING COMMITTEE:

Peter B. Flemings, Supervisor

Jacob A. Covault

Ann E. Cook

Hydrate-bearing sands in the Terrebonne Basin record the transition from ponded deposition to bypass in the deep-water Gulf of Mexico

by

Gabrielle Marie Varona

Thesis

Presented to the Faculty of the Graduate School of

The University of Texas at Austin

in Partial Fulfillment

of the Requirements

for the Degree of

Master of Science in Geological Sciences

The University of Texas at Austin

December 2022

Acknowledgements

First, I would like to thank my advisor, Peter Flemings, for his extraordinary guidance. He never failed to push me because he knew what I was capable of. As his student, I am amazed at how much we accomplished in the longest yet shortest two and half years of my life. Peter always challenged my perspective, thus allowing me to learn how to defend and build confidence in my interpretations. Peter is truly one of a kind, and I feel so honored that I was able to learn and grow not only as a geoscientist but as a person venturing off into the next chapter of my life. Without him, none of this would have been possible, and I am forever grateful.

I would also like to thank my committee members, Jake Covault and Ann Cook, for their constructive feedback and guidance. Absorbing their insight and perspectives on geological processes allowed me to expand my mind and think critically. I would like to thank David Mohrig as well for always carving out time for me to pick his brain. I will miss our chats, but I am thankful I can fall back on them whenever I need to. And to Alexey Portnov, I'm so lucky to have collaborated with you.

Lastly, I would like to thank those in my life that have been there from the start. My incredible parents, Mike and Maria Varona, for their unconditional love and support as I pursue my dream. My brother, Rafael Varona, for his encouragement. Susan Forthuber, for sharing her world with me and setting me off an adventure that I will never regret. John Austin, for welcoming a young geoscientist and bringing me back to the University of Texas. Finally, my two best friends, Brooke Kopecky and Colt Kernan, for always staying by side. Our friendship has gotten me through the moments where I doubted myself. Thank you all for bringing the joy that gets me through my days.

Abstract

Hydrate-bearing sands in the Terrebonne Basin record the transition from ponded deposition to bypass in the deep-water Gulf of Mexico

Gabrielle Marie Varona. M.S. Geo. Sci.

The University of Texas at Austin, 2022

Supervisor: Peter B. Flemings

Herein, I show how seismic stratigraphy can be used to describe the transition from ponded deposition to bypass within a gas hydrate system in deep-water Gulf of Mexico. In Walker Ridge Block 313 (WR 313), the Green and Orange sands are gas hydrate bearing sheet sands incised by a paleo channel system within the southwestern lobe of the Terrebonne Basin. I discuss two intervals that characterize the deposition of the sheet sands in conjunction with the channel. The Green interval captures the first appearances of coarse-grained material which I classify as the Green sand. The Orange interval encompasses channelized deposits and corresponding muddy levee deposits and is capped by the Orange sand. Within WR 313, the channel is oriented NW-SE and flowed towards the SE where salt related uplift took place. During the Green interval, salt movement influenced the pattern of deposition upstream and incision downstream. During the Orange interval, the channel aggraded, encountered the sheet deposition of the Orange sand, and then shut off. Well log data from two different wells support my interpretation of the Green and Orange sands as sheet sands due to their thickness patterns ~2000 m away from the

channel axis. The WR 225 001 (WR 225-1) well penetrates the Green and Orange deposits upstream and the WR 313 H001 (WR 313-H) well encounters these deposits downstream. The gamma ray and resistivity logs from the WR 225-1 well record two coarsening upward signatures several meters apart which are interpreted as the Green sand (74 meters thick) and the Orange sand (22 meters thick). I correlate these gamma ray signatures with thinner packages of the Green sand (35 meters) and the Orange sand (12 meters) in the WR 313-H well on the downstream end. Due to the thickness of the sands away from the channel and the corresponding seismic character, I interpret that the Green and Orange sands record the last episodes of high energy deposition that interact with a submarine channel system.

Table of Contents

List of Figures 9

Chapter 1: Introduction 17

1.1 Objectives 17

1.2 Overview 18

Chapter 2: Hydrate-bearing sands in the Terrebonne Basin record the transition from ponded deposition to bypass in the deep-water Gulf of Mexico 20

Abstract 20

2.1 Introduction 21

2.2 Geologic Background 25

2.2.1 Geologic Setting 25

2.2.2 Previous Work 25

2.3 Data and Methods 27

2.3.1 Wells and Seismic 27

2.3.2 Methods 28

2.4 Results 30

2.4.1 Seismic Characterization of the Green and Orange Intervals 30

2.4.2 Log Characterization of the Green and Orange Intervals 39

2.5 Discussion 43

2.5.1 Interpretation of the Green and Orange Intervals 43

2.5.2 Implications for the Hydrate Reservoir 49

2.6 Conclusions 50

2.7 Acknowledgements 51

2.8 Funding 51

Chapter 3: Appendix 52

Appendix A: Instantaneous Amplitude Maps of the Purple and Base Green Horizons 52

Appendix B: Difference Maps 55

References 59

List of Figures

Figure 1. (a) The Terrebonne Basin is a salt-confined minibasin. The study area is highlighted by the red box in 1a, and is located in the (b) SW lobe (portion) of the Terrebonne Basin. The 3D Depth (b, dashed box) and 3D Time (a, dashed line) seismic surveys along with well log data ('circles' (surface location) and '+' (bottomhole location)) were used to characterize and interpret the Top Green and Orange horizons. 23

Figure 2. (previous page) (a) Uninterpreted and (b) interpreted seismic sections through the Terrebonne Basin (located in Figure 1b). Multiple dipping horizons cross the base of hydrate stability zone (BHSZ) within the study area. Three wells in WR 313 intersect the horizons above and below the BHSZ (green curve = gamma ray, red curve = resistivity). We define the BHSZ as the surface above which hydrate is stable and below which it is not. The BHSZ is mapped as a discontinuous bottom simulating reflector (BSR) in Terrebonne (Hillman et al., 2017). The inset (a) illustrates that the horizon when above the BHSZ was mapped on the peak amplitude, whereas when the horizon was below the BHSZ, the horizon was mapped on the trough amplitude. The Top Green and Orange horizons have been previously mapped and are interpreted to contain gas hydrate (Boswell et al., 2012; Frye et al., 2012; Meazell and Flemings, 2022). 25

Figure 3. (previous page) Seismic cross section B-B’ (location in Figure 1b) showing a downstream cut of the channel. (a) Seismic section with Purple horizon displayed (negative polarity reflection). (b) Seismic section B-B' flattened along the Purple horizon; the channel features are more apparent. Windows, shown in yellow, are used to calculate Root Mean Square (RMS) amplitude attribute presented in Figure 7. (c) Interpreted seismic section B-B' with the mapped horizons discussed in this paper: Purple, Base Green, Top Green, and Orange. The black dashed line represents an interpreted erosional surface. The Green interval (GI) spans the Base Green and Top Green horizons. The Orange interval (OI) spans the Top Green and Orange horizons. The WR 313-H (gamma ray (green) and resistivity (red) curves displayed) well penetrated the Top Green and Orange horizons to the NE flank of the channel. 30

Figure 4. Instantaneous amplitude at the Top Green horizon. Contours are in meters below sea level (mbsl) (CI = 200 meters). The amplitude extraction north of the red outline (3D Depth Seismic Extent) was taken on the 3D time dataset. The channel axis is interpreted with the white dashed line and trends NW-SE within the 3D Depth Seismic Extent. The base of hydrate stability zone (BHSZ) is mapped as the pink dashed line. Below the BHSZ, the Top Green horizon is mapped on a trough amplitude. Above the BHSZ, the Top Green horizon is mapped on a peak amplitude. The red outline shows the extent of the 3D depth survey, brown lines show lease block boundaries, white circles show surface location of wells. 31

Figure 5. Instantaneous amplitude at the Orange horizon. Contours are in meters below sea level (mbsl) (CI = 200 meters). The amplitude extraction past the red outline (3D Depth Seismic Extent) was taken on the 3D time dataset. The channel axis is interpreted in the white dashed line and trends NW-SE within the 3D Depth Seismic Extent. Below the base of hydrate stability zone (BHSZ), the Orange horizon is mapped on a trough amplitude. Above the BHSZ, the Orange horizon is mapped on a peak amplitude. Red outline shows extent of the 3D depth survey, brown lines show lease block boundaries, white circles show surface location of wells. 33

Figure 6. (a) Thickness map of the Purple to Top Green horizons (CI = 50 m). Brown lines show lease block boundaries and white circle shows surface location of WR 313-H. (b) On the upstream end, the channel incises into the Top Green horizon. (c) On the downstream end, the channel incises the Top Green and Base Green horizons and into the underlying strata. The degree of incision is greater on the downstream end (c) compared to the upstream end (b).....34

Figure 7. RMS amplitude maps of (a) Window A, (b) Window B, and (c) Window C. (d) Schematic cartoon showing the RMS windows in relation to the Green and Orange intervals. In all three RMS amplitude maps, the channel trends NW-SE. In (a) Window A, high amplitude, discontinuous 'kidney bean' shaped features are within the main channel belt and appear to flank either side of the respective, low amplitude thalweg. The larger loop like feature is truncated by the low amplitude thalweg. In (b) Window B and (c) Window C, the channel appears to straighten. Generally, the high amplitude features are restricted within the channel belt (Window A) or flank either side of the thalweg (Windows B and C). ..36

Figure 8. (previous page) a) and b): Seismic and line drawing interpretation for upstream (A-A') and downstream locations (C-C') locations. Sections are located on Figure 4. (b and c) The Green interval is highlighted in light green and the Orange interval is highlighted in orange. Upstream (a and b), several 'u-shaped' seismic reflections link to 'wing-like' linear features that stack on top of each other through the Orange interval. Downstream (c and d), the Top Green and Base Green horizons are truncated by an erosional boundary (dashed line) which is then filled in with u-shaped seismic reflections. These reflections stack on top of each other and link with wing-like reflections outside of the boundary. At the top of the Orange interval, the Orange horizon is a regional prominent reflector but is locally absent within the channel.....39

Figure 9. Well logs for WR 313-H of the Green and Orange sands (highlighted in yellow). The top of the Green sand corresponds to a negative polarity reflection (mapped as the Top Green horizon) and the base of the Green sand corresponds to a positive polarity reflection (mapped as the Base Green horizon). The top of the Orange sand corresponds to a positive polarity reflection (mapped as the Orange horizon) at this location (Figure 5) since it is above the BHSZ. Due to the response in velocity and density at the Orange sand, we interpret that the Orange sand contains gas hydrate. 40

Figure 10. Stratigraphic cross section (located on Figure 5) of the Orange sand, Green sand, and Purple equivalent (hung on the top of the Orange sand). Within the main study area, this cross section captures the sands to the NE of the central channel axis (Figure 5). The Green and Orange sands thin from the north to the southeast. We interpret that the Orange sand is eroded within the WR 313-G well. Both the Green and Orange sands are significantly thicker in the northern portion of the basin and we interpret that they are unrelated to channelized deposition. 42

Figure 11. Simplified line drawing evolution of the Green and Orange intervals on the (a) upstream and (c) downstream ends of the channel. Line drawings are based off of (b) upstream and (d) downstream seismic sections (location on Figure 4). The WR 313-H (gamma ray (green) and resistivity (red) log curves displayed) well penetrated the Top Green and Orange and horizons to the NE flank of the channel. On the (b) upstream end, several u-shaped seismic reflections are flanked by wing-like reflections that stack on top of each other from the Base Green to the Orange horizons. On the (d) downstream end, the Top Green and Base Green horizons are truncated by a boundary marked by the dashed line that signifies the end of the Green interval. The dashed line is then filled in by several u-shaped reflections that stack on top of each other. The u-shaped reflections are then flanked by wing-like reflections outside of the boundary until they encounter Orange horizon. This geometry is maintained in the upstream and downstream sections until the channel shuts off and is blanketed by a continuous seismic event.....47

Figure 12. (previous page) Interpreted 2D line (left) and corresponding map view (right) of the evolution of the submarine channel system in the southwestern lobe of the Terrebonne Basin. (a) (T=1) Turbulent flows enter the southwestern lobe of Terrebonne depositing sheet-like sands coincidentally with active salt movement. We interpret a knickpoint initiates, propagates to the upstream end, and a bypass surface develops. b) (T=2) The Top Green Hz marks the end of the Green interval. The Green sand (GS) consists of the coarser material stripped from the turbulent flows that were deposited during the Green interval. c) (T=3) After the Green interval, the channel transitions from a bypass phase to a depositional phase (the beginning of the Orange interval). d) (T=4) During the Orange interval, the channel aggrades on both the upstream and downstream ends until the deposition of the Orange sand (OS) (top of Orange sand correlates to the Orange Hz). e) (T=5) After the deposition of the Orange interval, the channel incises the Orange Hz and continues to aggrade until it shuts off. 49

Figure A1. Instantaneous amplitude at the Purple horizon. Contours are in meters below sea level (mbsl) (CI = 200 meters). The amplitude extraction north of the red outline (3D Depth Seismic Extent) was taken on the 3D time dataset. The red outline shows the extent of the 3D depth survey, brown lines show lease block boundaries, white circles show surface location of wells. 53

Figure A2. Instantaneous amplitude at the Base Green Horizon. Contours are in meters below sea level (mbsl) (CI = 200 meters). The amplitude extraction north of the red outline (3D Depth Seismic Extent) was taken on the 3D time dataset. The red outline shows the extent of 3D depth survey, brown lines show lease block boundaries, white circles show surface location of wells. 54

Figure B1. (a) Thickness map of the Purple to Base Green horizons (CI = 25 m). Brown lines show lease block boundaries and white circle shows surface location of WR 313-H. (b) On the upstream end, the Base Green is continuous from SW to NE; there is no obvious channelized incision. (c) On the downstream end, the channel incises the Base Green horizon and the underlying strata.....56

Figure B2. Regional thickness map of the Purple to Top Green horizons (CI = 50 m). Brown lines show lease block boundaries and white circle shows surface locations of wells. Red outline shows the 3D depth seismic data extent.....57

Figure B3. Regional thickness map of the Top Green to Orange horizons (CI = 50 m). Brown lines show lease block boundaries and white circle shows surface locations of wells. Red outline shows the 3D depth seismic data extent.....58

Chapter 1: Introduction

1.1 Objectives

Gas hydrate reservoirs have garnered plenty of interest in the past decade due to their abundance below the subsurface and their potential to be used as an unconventional energy resource (Boswell et al., 2012; Flemings et al., 2020; Frye et al., 2012). However, gas hydrates form in specific P/T conditions of high pressures and low temperatures; these conditions limit where gas hydrates tend to accumulate as well as their stability within a reservoir. Previous studies have identified, mapped, and characterized gas hydrate reservoirs around the world and more specifically within the northern Gulf of Mexico (Brooks et al., 1984; McConnell and Kendall, 2002; Milkov and Sassen, 2001). The mechanism for gas hydrate production is yet to be determined. Therefore, studying the stratigraphic elements of gas hydrate reservoirs is necessary to understand the lateral extent, potential drive mechanism, and connectivity of gas hydrate deposits for future production.

The main objectives of this work are to characterize the interaction of salt tectonism and sedimentary processes occurring in Walker Ridge Block 313 (WR 313) within the Terrebonne Basin, deep-water Gulf of Mexico, and propose a paleogeographic evolution of two gas hydrate reservoirs (the Green and Orange sands). McConnell and Kendall (2002) first identified gas hydrate potential within WR 313, and Boswell et al. (2012) and Frye et al. (2012) discuss the architectural elements of gas hydrate reservoirs within this area. Boswell et al. (2012) and Frye et al. (2012) describe and interpret the depositional history of two gas hydrate bearing reservoirs (the Green sand and the Orange sand) associated with a submarine channel system. I am interested in the Green and Orange sands

and their interaction with the submarine channel system to understand their overall reservoir extent within the Terrebonne Basin and their implications for future work.

1.2 Overview

In Chapter 2, I present a paleogeographic evolution of the Green and Orange Sands in the Terrebonne Basin. I integrate expanded depth- and time-migrated 3D seismic reflection data with well log data located within the broader Terrebonne Basin, to extend the initial interpretations of the Green and Orange sands away from the local study area (WR 313) of Boswell et al. (2012) and Frye et al. (2012). Within WR 313, the Green and Orange sands flank either side of a submarine channel system and are coarser-grained away from the channel axis. With the expanded data, I observe that the Green and Orange sands are laterally continuous away from the submarine channel and significantly thicken from upstream to downstream. These observations are characterized by a submarine depositional system that describes unconfined accumulation of coarse-grained material (sheet-like sands) incised by a submarine channel system within a sedimentary basin. This type of system is recognized within basins around the world (e.g. Flint et al. (2011) and Jobe et al. (2017)) and specifically within the Gulf of Mexico, where Prather et al. (2012) classifies this system as a 'perched slope apron.' Thus, I propose that the Green and Orange sands are sheet sands that were incised by a submarine channel in a perched slope apron depositional setting. I interpret that the Green and Orange sands represent the last phases of high energy deposition within the Terrebonne Basin, before the system transitioned to bypass.

This interpretation implies that the Green and Orange sands increase in reservoir quality away from the channel axis due to their initial unconfined deposition. Within the channel axis, I predict compartmentalization of or a lack of the Green and Orange sands as

I expect them to be reworked or completely eroded. In the future, the Orange sand will be drilled and cored away from channel axis. I predict that the Orange sand will be coarse grained in this location based on the observations and interpretations described above and further within Chapter 2. Chapter 2 will be submitted for future publication.

Appendices in Chapter 3 contain additional maps that were generated to support the interpretations described in Chapter 2. The appendices include A) instantaneous amplitude maps of the Purple and Base Green horizons and B) additional thickness maps within the Green and Orange intervals.

Chapter 2: Hydrate-bearing sands in the Terrebonne Basin record the transition from ponded deposition to bypass in the deep-water Gulf of Mexico

ABSTRACT

Herein, we show how seismic stratigraphy can be used to describe the transition from ponded deposition to bypass within a gas hydrate system in deep-water Gulf of Mexico. In Walker Ridge Block 313 (WR 313), the Green and Orange sands are gas hydrate bearing sheet sands incised by a paleo channel system within the southwestern lobe of the Terrebonne Basin. We discuss two intervals that characterize the deposition of the sheet sands in conjunction with the channel. The Green interval captures the first appearances of coarse-grained material which we classify as the Green sand. The Orange interval encompasses channelized deposits and corresponding muddy levee deposits and is capped by the Orange sand. Within WR 313, the channel is oriented NW-SE and flowed towards the SE where salt related uplift took place. During the Green interval, salt movement influenced the pattern of deposition upstream and incision downstream. During the Orange interval, the channel aggraded, encountered the sheet deposition of the Orange sand, and then shut off. Well log data from two different wells support our interpretation of the Green and Orange sands as sheet sands due to their thickness patterns ~2000 m away from the channel axis. The WR 225 001 (WR 225-1) well penetrates the Green and Orange deposits upstream and the WR 313 H001 (WR 313-H) well encounters these deposits downstream. The gamma ray and resistivity logs from the WR 225-1 well record two coarsening upward signatures several meters apart which are interpreted as the Green sand (74 meters thick) and the Orange sand (22 meters thick). We correlate these gamma ray signatures with thinner packages of the Green sand (35 meters) and the Orange sand (12 meters) in the WR 313-H well on the downstream end. Due to the thickness of the sands

away from the channel and the corresponding seismic character, we interpret that the Green and Orange sands record the last episodes of high energy deposition that interact with a submarine channel system.

2.1 INTRODUCTION

Salt tectonism in conjunction with sedimentation has created the stratigraphic architecture of minibasins within the northern Gulf of Mexico (Diegel et al., 1995; Worrall and Snelson, 1989). Over the last 30 years, our understanding of the forces that drive minibasin evolution have advanced. A general conceptual model has developed wherein sands fill in the accommodation created by salt withdrawal and ultimately when this accommodation is exhausted, sediment can bypass and exit the minibasin through submarine channels that transport coarser grained material farther downdip (Deptuck et al., 2012; Jobe et al., 2017; Prather et al., 2012). At the largest scale this results in a stratigraphic architecture that is sand rich and dominated by large regional sheet sand deposits that are ultimately overlain by channelized deposition grading into a sand-poor interval that records bypass (Booth et al., 2003; Prather et al., 2012). Reconstructing the interactions between sheet-like sands and submarine channel deposits allow us to understand the connectivity and lateral extent of coarse-grained reservoirs that fill in minibasins throughout the northern Gulf of Mexico.

Gas hydrates have the potential to serve as an unconventional energy resource due to the large amount of gas present and their abundance below the subsurface (Boswell et al., 2012; Flemings et al., 2020; Frye et al., 2012). Previous studies have mapped and identified hydrate reservoirs within the sand deposits that fill minibasins throughout the Gulf of Mexico (Brooks et al., 1984; McConnell and Kendall, 2002; Milkov and Sassen, 2001). For example, within Alaminos Canyon Block 21 (AC 21), Boswell et al. (2012)

interprets a hydrate-bearing sand-rich mass transport deposit (MTD) or basin floor fan that fills the accommodation of the Diana minibasin. At Green Canyon Block 955 (GC 955), along the edge of the Sigsbee Escarpment, leveed-channel deposits were mapped, logged, and cored and found to contain high saturation hydrate within a sandy-silt matrix (Flemings et al., 2020; Meazell et al., 2020; Santra et al., 2020).

An area that has received particular attention, but has not yet been cored is the Terrebonne Basin. In this salt confined minibasin, gas hydrates have been encountered within sand deposits that interact with a submarine channel-levee system (Boswell et al., 2012; Frye et al., 2012; Hutchinson et al., 2009). Two interpretations have developed regarding the depositional environment and the geometry of these sand bodies (e.g. Boswell et al. (2012) and Frye et al. (2012)). However, these interpretations were limited due to the seismic data extent at the time and the depositional models never fully explained the coarse-grained nature of the hydrate-bearing reservoirs far away from the channel axis.

In this paper, we examine the overall evolution of the Terrebonne Basin and then focus on two hydrate-bearing reservoirs, the Green and Orange sands. We integrate seismic reflection data and log data to describe the stratigraphic evolution of this system. We ultimately interpret that the Green and Orange sands represent the final stages of minibasin fill in the Terrebonne Basin. The Green and Orange sands record the transition from deposition to bypass on the basin scale. Importantly, we interpret that both the Green and Orange sands are high energy sheet sand deposits that span the Terrebonne Basin and were incised by the submarine channel system. As such, they are more laterally continuous and potentially of coarser grain size compared to previously cored hydrate leveed-channel deposits.

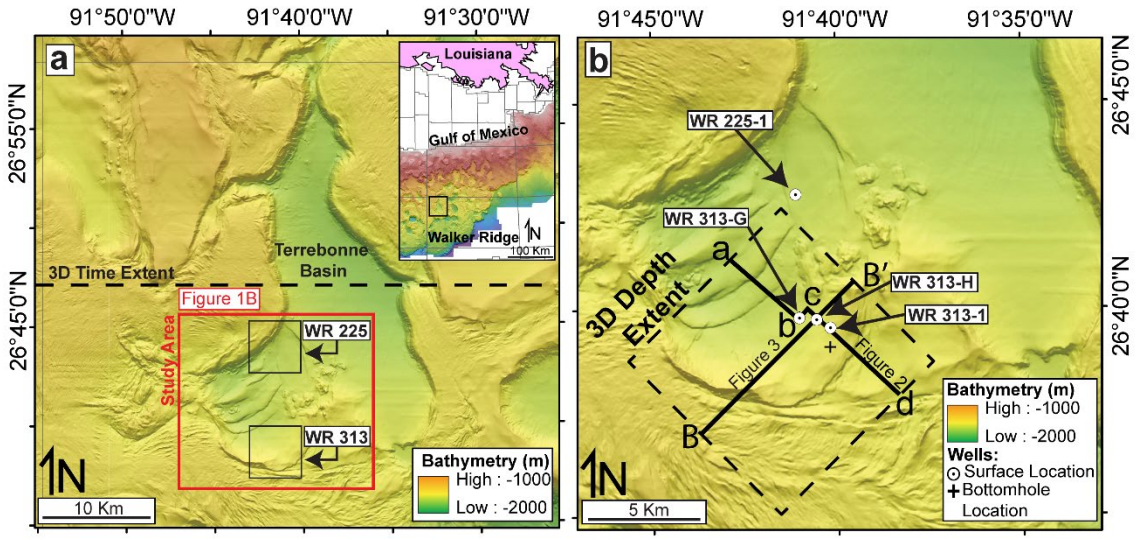

Figure 1. (a) The Terrebonne Basin is a salt-confined minibasin. The study area is highlighted by the red box in 1a, and is located in the (b) SW lobe (portion) of the Terrebonne Basin. The 3D Depth (b, dashed box) and 3D Time (a, dashed line) seismic surveys along with well log data ('circles' (surface location) and '+' (bottomhole location)) were used to characterize and interpret the Top Green and Orange horizons.

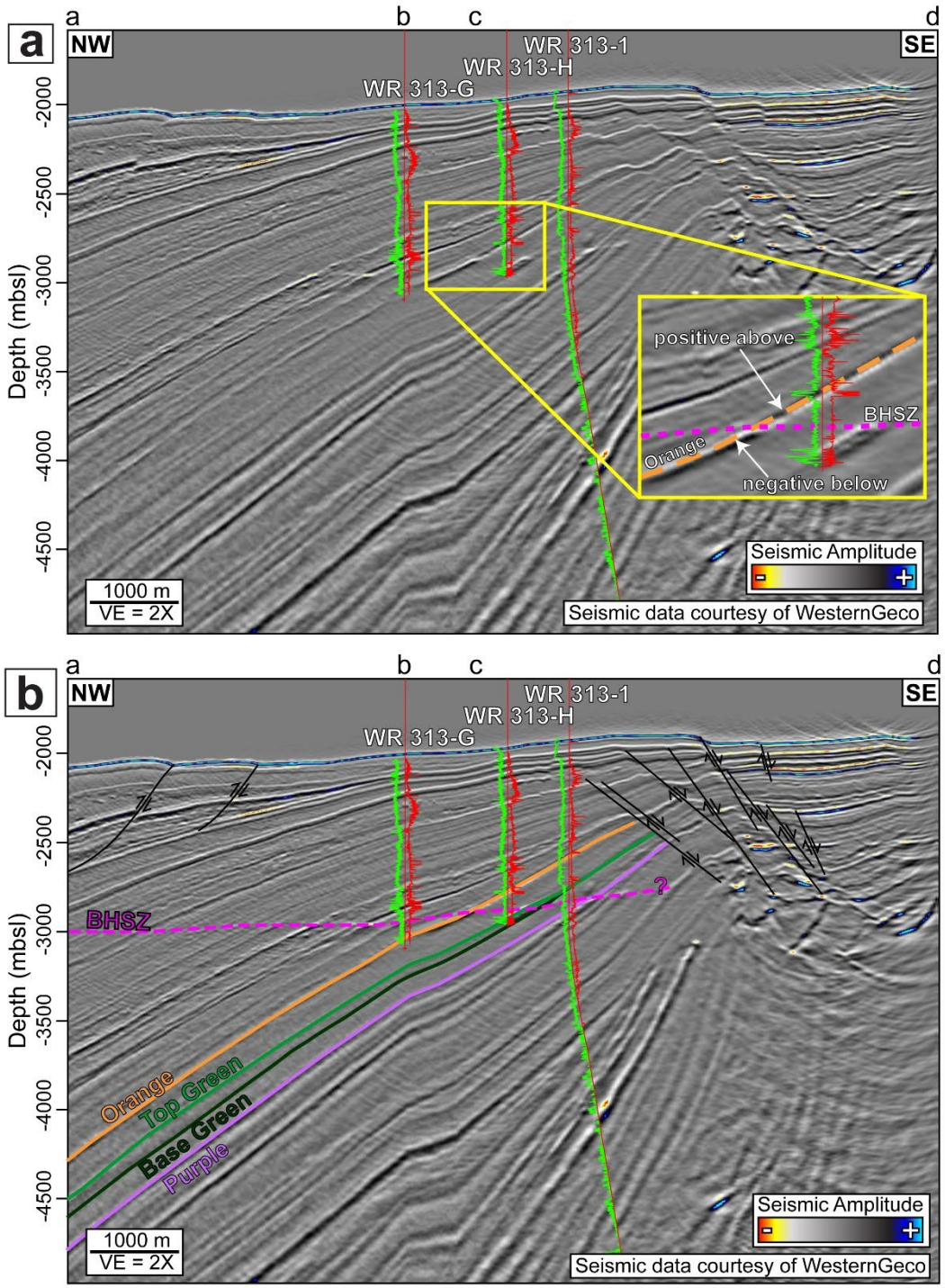
a
b
c
d
NW
SE
WR 313-1
WR 313-H
WR 313-G
Depth (mbsl)
-2000
-2500
-3000
-3500
-4000
-4500
positive above
BHSZ
Orange
negative below
Seismic Amplitude
1000 m
VE = 2X
Seismic data courtesy of WesternGeco
b
NW
SE
WR 313-1
WR 313-H
WR 313-G
BHSZ
?
Orange
Top Green
Base Green
Purple
Seismic Amplitude
1000 m
VE = 2X
Seismic data courtesy of WesternGeco

Figure 2. (previous page) (a) Uninterpreted and (b) interpreted seismic sections through the Terrebonne Basin (located in Figure 1b). Multiple dipping horizons cross the base of hydrate stability zone (BHSZ) within the study area. Three wells in WR 313 intersect the horizons above and below the BHSZ (green curve = gamma ray, red curve = resistivity). We define the BHSZ as the surface above which hydrate is stable and below which it is not. The BHSZ is mapped as a discontinuous bottom simulating reflector (BSR) in Terrebonne (Hillman et al., 2017). The inset (a) illustrates that the horizon when above the BHSZ was mapped on the peak amplitude, whereas when the horizon was below the BHSZ, the horizon was mapped on the trough amplitude. The Top Green and Orange horizons have been previously mapped and are interpreted to contain gas hydrate (Boswell et al., 2012; Frye et al., 2012; Meazell and Flemings, 2022).

2.2 GEOLOGIC BACKGROUND

2.2.1 Geologic Setting

The Terrebonne Basin is a salt-confined minibasin within the middle slope of the tabular salt and minibasin province of the northern Gulf of Mexico (Diegel et al., 1995) in the Walker Ridge protraction area (Figure 1a) (Frye et al., 2012). Within the southwestern lobe, Terrebonne is bounded by areas of elevated bathymetry caused by salt movement (Figure 1b). Hydrate-bearing seafloor mounds, described by McConnell and Kendall (2002) and Meazell and Flemings (2022), are prominent bathymetric features (Figure 1b). Several thrust faults (Figure 2) displace strata to the northwest of the study area and are expressed along the seafloor (Figure 1b). Strata onlap salt towards the southeast and dip northwest (Figure 2).

2.2.2 Previous Work

McConnell and Kendall (2002) first identified and described gas hydrate potential in WR 313 after they observed seismic discontinuities that could be linked together at the base of hydrate stability zone (BHSZ) (Frye et al., 2012; McConnell and Kendall, 2002) (Figure 2). The BHSZ marks the boundary above which hydrate is stable and below which

hydrate is not stable (Frye et al., 2012). Above the BHSZ, the presence of hydrate results in a high acoustic impedance due to the high velocity of the hydrate; the contrast between hydrate above and gas or water below is imaged as a positive polarity reflection (peak) (Figure 2a, inset) (McConnell and Zhang, 2005). If gas is present below the BHSZ, then the contrast in acoustic impedance is further accentuated (Figure 2a, inset) (McConnell and Zhang, 2005). Thus, within a single horizon, the change in acoustic impedance from a negative polarity reflection (trough) to a positive polarity reflection (peak) can be mapped as the BHSZ (Figure 2a, inset) (Hillman et al., 2017; McConnell and Kendall, 2002; Shedd et al., 2012).

Three wells were drilled in WR 313. The WR 313 001 (OCS-G 18683 #001; referred to as WR 313-1 in this paper) was drilled by Ocean Energy in 2001 in the southeastern margin of the study area (Figure 1b) and targeted Pliocene and Miocene oil reservoirs in the Titan South prospect (Frye et al., 2012). In 2009, the Gas Hydrate Joint Industry Project (JIP) conducted a logging while drilling (LWD) expedition (Boswell et al., 2012; Frye et al., 2012; Hutchinson et al., 2009). The WR 313 G001 (WR 313-G) and WR 313 H001 (WR 313-H) wells were drilled to test gas hydrate targets.

The Green and Orange sands were mapped by Frye et al. (2012) and Boswell et al. (2012) in WR 313 (Figure 2b). The WR 313-G, -H, and -1 wells penetrate gas hydrate bearing layers on the northeastern flank of the channel. The WR 313-H well intersects the Green sand below the BHSZ and did not measure gas hydrate or free gas. At the WR 313-1 well, the Green sand is composed of thin, hydrate-bearing layers (Frye et al., 2012). Frye et al. (2012) interpreted the Green sand as a series of stacked turbidite sheet sands deposited on the minibasin floor whereas Boswell et al. (2012) interprets this sand as a levee flanking a turbidite channel. The overlying Orange sand is 8-m thick and contains hydrate at WR 313-H; the equivalent interval in WR 313-G is a water-saturated mudrock. Frye et al.

(2012) interprets that the Orange sand was deposited by low concentration turbidity currents in a partially confined basin setting. They interpret the clay-rich interval within WR 313-G is part of a mud rich channel that eventually coalesces with the main channel (Frye et al., 2012). In contrast, Boswell et al. (2012) interprets the Orange sand as a proximal levee flanking a turbidite channel.

2.3 DATA AND METHODS

2.3.1 Wells and Seismic

We use log data from the WR 313-1, -G, and -H and WR 225 001 (WR 225-1) (Figure 1B) wells. We use the gamma ray and resistivity logs to interpret sediment lithology and the compressional velocity and bulk density logs for constructing synthetic seismograms for seismic-well ties. We use proprietary depth-migrated and public time-migrated 3D seismic reflection data for mapping and interpretation of channel stratigraphy (Figure 1b). The depth-migrated 3D data were acquired in 2006-2007 by WesternGeco and processed using standard industry protocol followed by Kirchoff migration. Three-dimensional seismic data are sampled to 16 ft (4.87 m) and have 30/6.25 m inline/crossline intervals. The data limit of the depth-migrated 3D survey is shown in Figure 1b. The 3D time-migrated data were downloaded from NAMSS – National Archive of Marine Seismic Surveys and were used to extend our interpretation from the original depth-migrated 3D survey extent (dashed box, Figure 1b). The sampling rate of time-migrated data is 8 msec, the signal frequency range is 5-45 Hz, and the bin size is 20x25 meters. To identify the Top Green and Orange horizons in the time-migrated 3D seismic data, we visually correlate stratigraphy in both domains; we then use seismic-well tie at the WR 313-H well to verify our horizon picks. Finally, we use the 3D time-migrated data in conjunction with the WR 225-1 well to correlate the Top Green and Orange horizons from the original extent to the

north, into the broader Terrebonne Basin (Figure 1b). All seismic data are zero phase where the seafloor (positive reflection coefficient) is represented by a positive polarity reflection.

2.3.2 Methods

We mapped the Purple, Base Green, Top Green, and Orange horizons (Figure 3c). The Top Green and Orange horizons were mapped on a negative polarity reflection below the BHSZ and a positive polarity reflection above the BHSZ as described by Frye et al. (2012) and Meazell and Flemings (2022) (Figure 2a, inset). An erosional surface was also mapped as represented by the black dashed line in Figure 3c. In this paper, we discuss two intervals: the Green interval and the Orange interval. The Green interval is bounded below by the Base Green horizon and above by the Top Green horizon (Figure 3c). The Orange interval is bounded below by the Top Green horizon and above by the Orange horizon (Figure 3c).

We created instantaneous amplitude maps of the Top Green (Figure 4) and Orange (Figure 5) horizons. We generated a difference map between the Top Green and Purple horizons (Figure 6a) to observe the patterns in deposition within the Green interval (Figure 3c). To propose an evolutionary model of the channel system, we created proportional horizons within the Green and Orange intervals and used some of the horizons as boundaries for RMS amplitude windows (Figure 3b). Three RMS amplitude maps are discussed within this paper (Figure 7) and the corresponding RMS windows are displayed in Figure 3b.

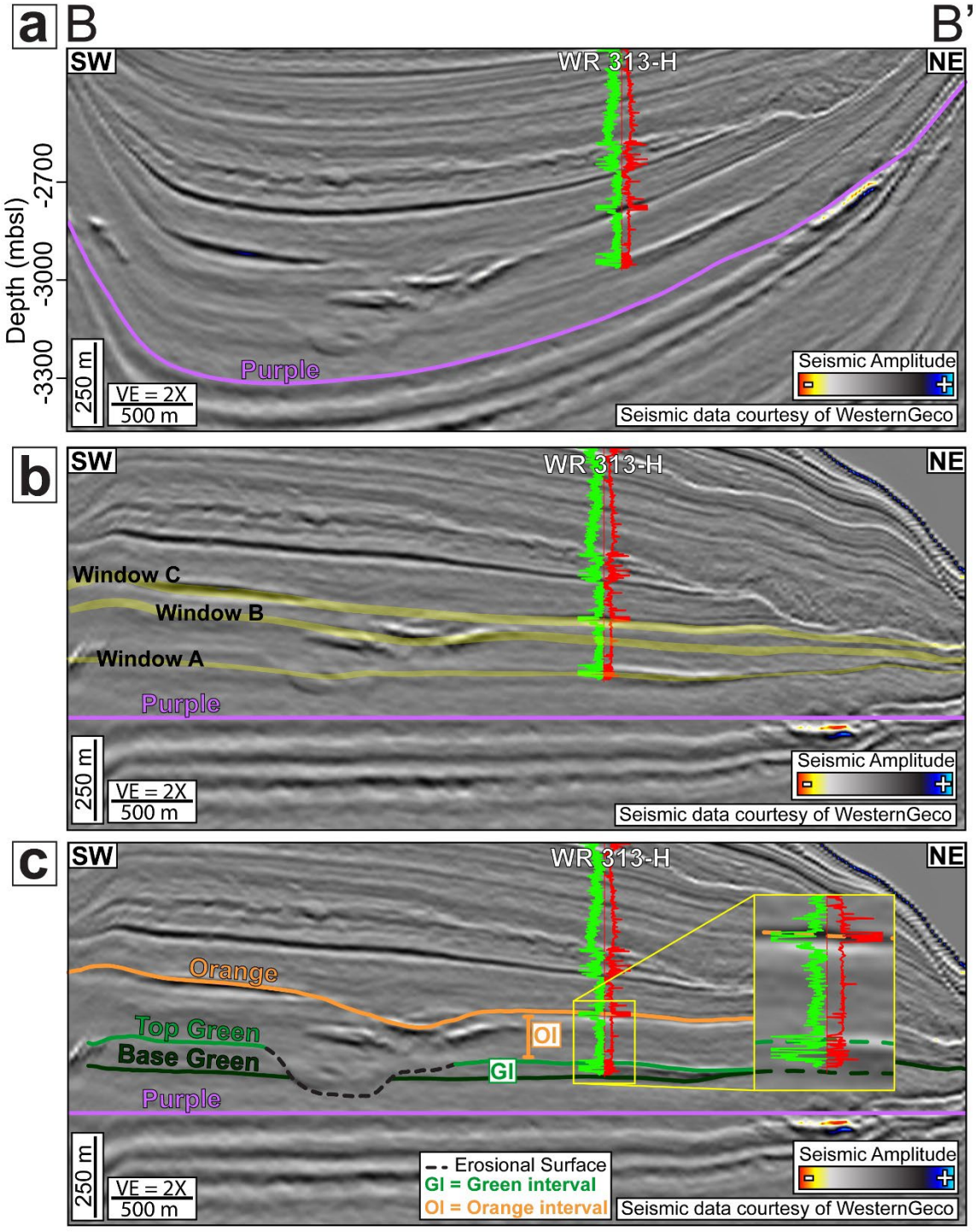
a
B
B'
SW
NE
WR 313-H
Depth (mbsl)
-2700
-3000
-3300
Purple
250 m
VE = 2X
500 m
Seismic Amplitude
Seismic data courtesy of WesternGeco
b
SW
NE
WR 313-H
Window C
Window B
Window A
Purple
250 m
VE = 2X
500 m
Seismic Amplitude
Seismic data courtesy of WesternGeco
c
SW
NE
WR 313-H
Orange
Top Green
Base Green
Purple
OI
GI
250 m
VE = 2X
500 m
Erosional Surface
GI = Green interval
OI = Orange interval
Seismic Amplitude
Seismic data courtesy of WesternGeco

Figure 3. (previous page) Seismic cross section B-B’ (location in Figure 1b) showing a downstream cut of the channel. (a) Seismic section with Purple horizon displayed (negative polarity reflection). (b) Seismic section B-B' flattened along the Purple horizon; the channel features are more apparent. Windows, shown in yellow, are used to calculate Root Mean Square (RMS) amplitude attribute presented in Figure 7. (c) Interpreted seismic section B-B' with the mapped horizons discussed in this paper: Purple, Base Green, Top Green, and Orange. The black dashed line represents an interpreted erosional surface. The Green interval (GI) spans the Base Green and Top Green horizons. The Orange interval (OI) spans the Top Green and Orange horizons. The WR 313-H (gamma ray (green) and resistivity (red) curves displayed) well penetrated the Top Green and Orange horizons to the NE flank of the channel.

2.4 RESULTS

2.4.1 Seismic Characterization of the Green and Orange Intervals

The Top Green horizon (Figure 4) has three distinguishing characteristics. First, there is a low amplitude linear feature interpreted as a submarine channel (Boswell et al., 2012; Frye et al., 2012) (‘Channel’, Figure 4) oriented NW-SE within WR 313 that is flanked by higher amplitudes that extend ~500 meters to the NE and ~1,000 meters to the SW. Second, there is a zone of high, negative amplitudes that parallel the structural contours and immediately underlie the BHSZ (pink dashed line, Figure 4). As described by Frye et al. (2012) and Meazell and Flemings (2022), these are interpreted to record free gas trapped beneath the base of the hydrate stability zone. Third, there is an abrupt contrast in seismic amplitude characterized by the BHSZ. Above the BHSZ, we interpret hydrate to be present.

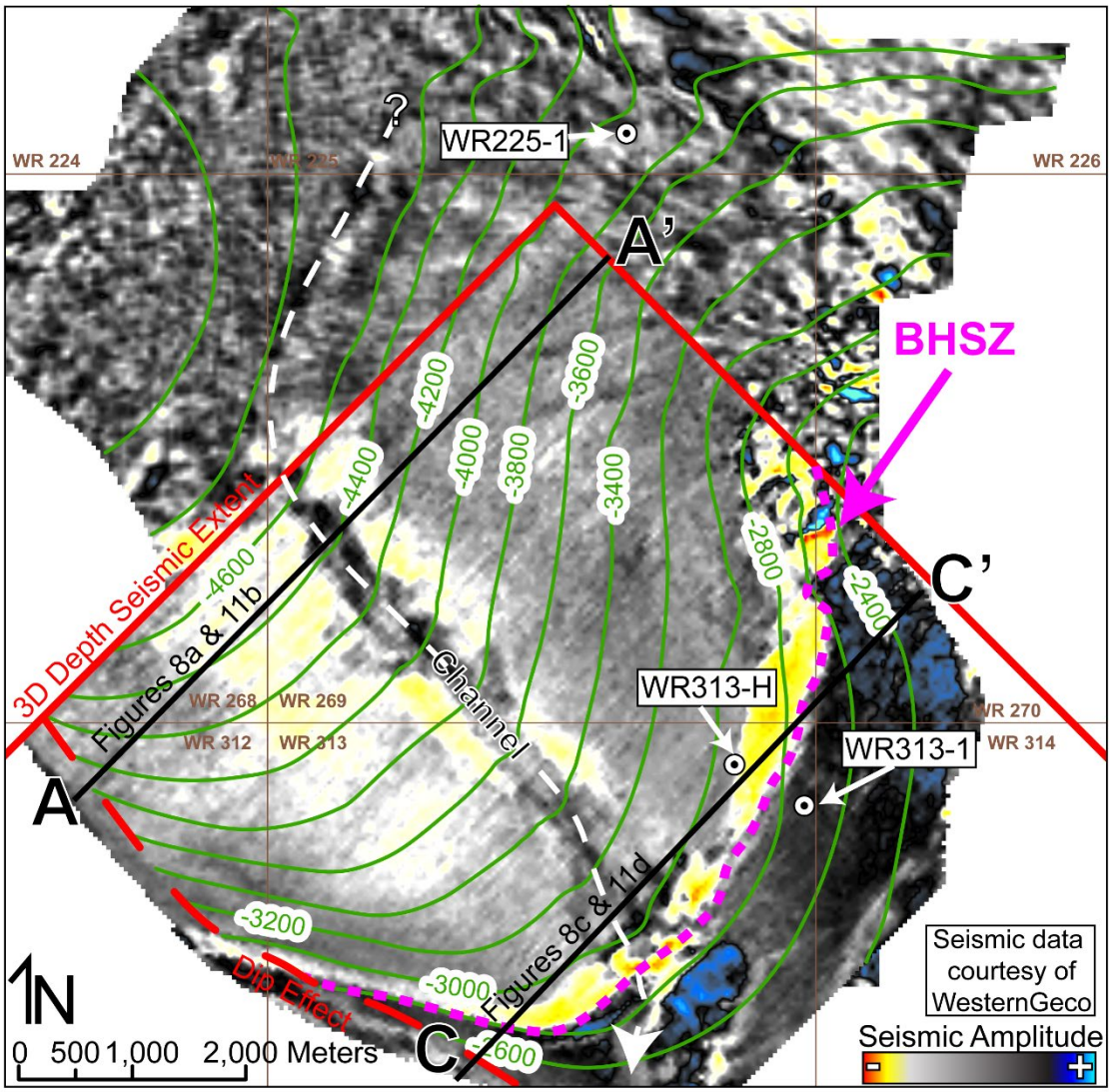

Figure 4. Instantaneous amplitude at the Top Green horizon. Contours are in meters below sea level (mbsl) (CI = 200 meters). The amplitude extraction north of the red outline (3D Depth Seismic Extent) was taken on the 3D time dataset. The channel axis is interpreted with the white dashed line and trends NW-SE within the 3D Depth Seismic Extent. The base of hydrate stability zone (BHSZ) is mapped as the pink dashed line. Below the BHSZ, the Top Green horizon is mapped on a trough amplitude. Above the BHSZ, the Top Green horizon is mapped on a peak amplitude. The red outline shows the extent of the 3D depth survey, brown lines show lease block boundaries, white circles show surface location of wells.

The Orange horizon (Figure 5) also has three distinguishing characteristics. First, the channel is still present ('Channel,' Figure 5) and is oriented NW-SE within WR 313. The channel is generally flanked by pockets of negative amplitude specifically towards the SW (Figure 5). Second, in the 3D depth seismic data, there are strong negative amplitudes both towards the NW corner of the map and down dip from the BHSZ. Meazell and Flemings (2022) interpreted the high amplitudes to the northwest as thick sand whereas the amplitudes downdip from the BHSZ are free gas. Third, there is a zone of dim amplitude response along the NE edge of the channel where the WR 313-G well is located (Figure 6). This dim zone is approximately 500 meters wide and extends ~2500 meters from NW-SE along the downstream edge of the channel.

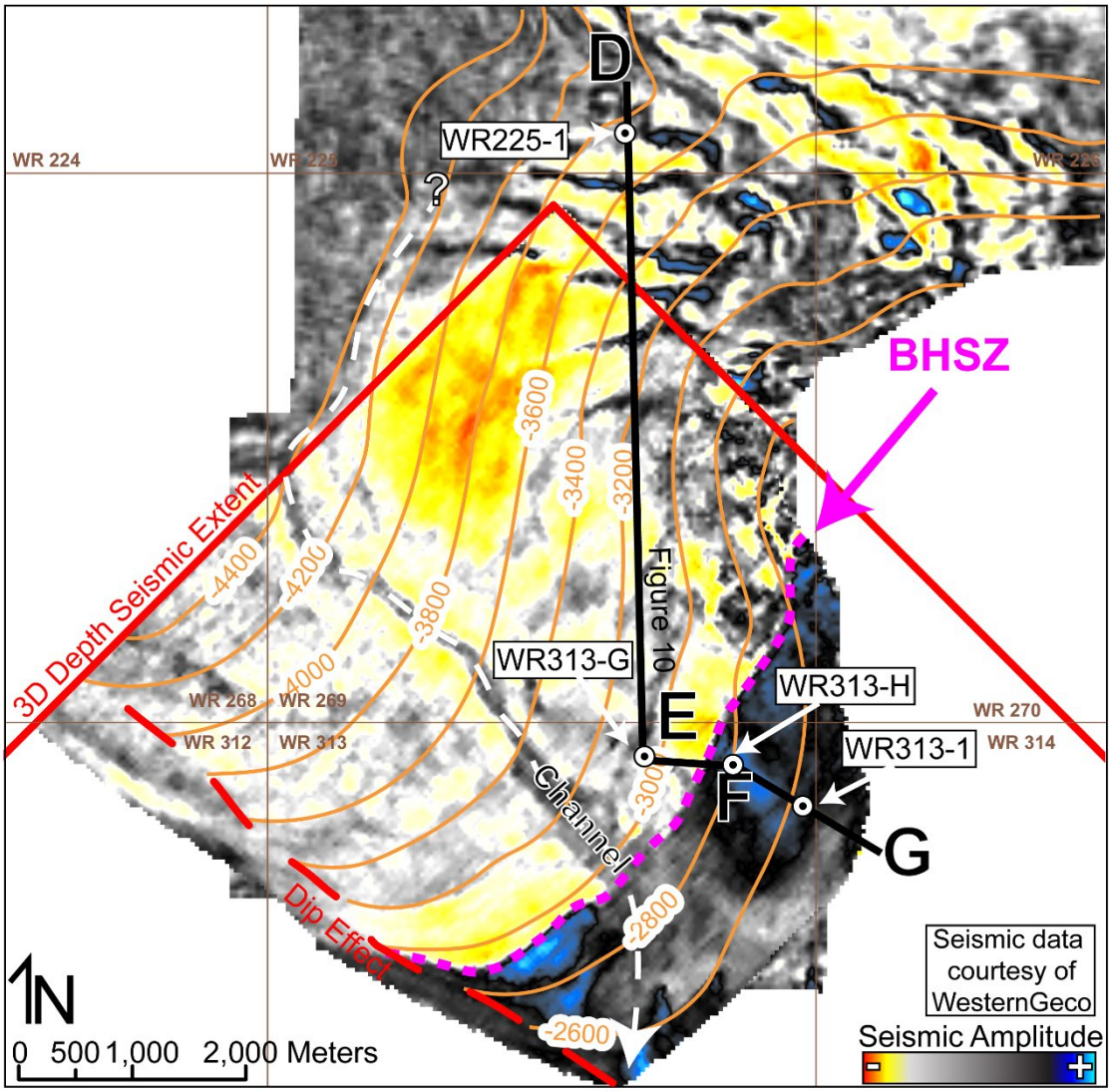

Figure 5. Instantaneous amplitude at the Orange horizon. Contours are in meters below sea level (mbsl) (CI = 200 meters). The amplitude extraction past the red outline (3D Depth Seismic Extent) was taken on the 3D time dataset. The channel axis is interpreted in the white dashed line and trends NW-SE within the 3D Depth Seismic Extent. Below the base of hydrate stability zone (BHSZ), the Orange horizon is mapped on a trough amplitude. Above the BHSZ, the Orange horizon is mapped on a peak amplitude. Red outline shows extent of the 3D depth survey, brown lines show lease block boundaries, white circles show surface location of wells.

An isopach map of the Purple to Top Green horizons is shown in Figure 6a. The channel previously observed in the Top Green (Figure 4) and Orange horizons (Figure 5) is characterized by thickness contours that 'v' towards the NW. The deposits flanking the NE side of the channel decrease in thickness from NW to SE (Figure 6a). Cross sections A-A' (Upstream, Figure 6b) and B-B' (Downstream, Figure 6c) compare the thickness between the Top Green, Base Green, and Purple horizons (the Green interval, Figure 3c). In the upstream cross section (Figure 6b), the Base Green is continuous from SW to NE while the Top Green horizon dips along the channel axis (Figure 6a). In the downstream cross section (Figure 6c), the Top Green horizon incises the Base Green horizon.

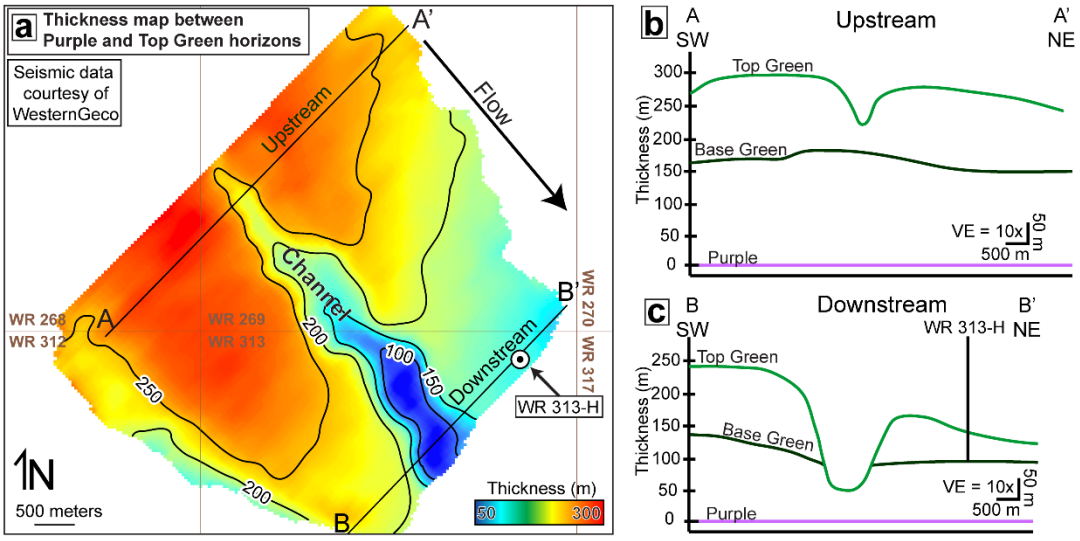

Figure 6. (a) Thickness map of the Purple to Top Green horizons (CI = 50 m). Brown lines show lease block boundaries and white circle shows surface location of WR 313-H. (b) On the upstream end, the channel incises into the Top Green horizon. (c) On the downstream end, the channel incises the Top Green and Base Green horizons and into the underlying strata. The degree of incision is greater on the downstream end (c) compared to the upstream end (b).

We generated three root mean square (RMS) amplitude maps (Figure 7) from surfaces within the Green and Orange intervals. Window A cross cuts the Green interval and the Orange interval (Figure 7d). This RMS amplitude map (Figure 7a) shows pockets of high amplitude ('kidney bean' shaped features) that trend NW-SE and flank the channel. A large loop like feature is captured towards the northwest end of the channel. Window B is within the Orange interval (Figure 7d). In this RMS map (Figure 7b), the channel is straighter compared to Window A and the high amplitudes that flank the channel follow its geometry. Window C is within the top portion of the Orange interval (Figure 7d). The corresponding RMS amplitude map (Figure 7c) shows that the channel has less sinuosity compared to Window B and the higher amplitudes that flank the channel also decrease in sinuosity. The overall presence of higher amplitudes increases in Figure 7c but are discontinuous throughout the map.

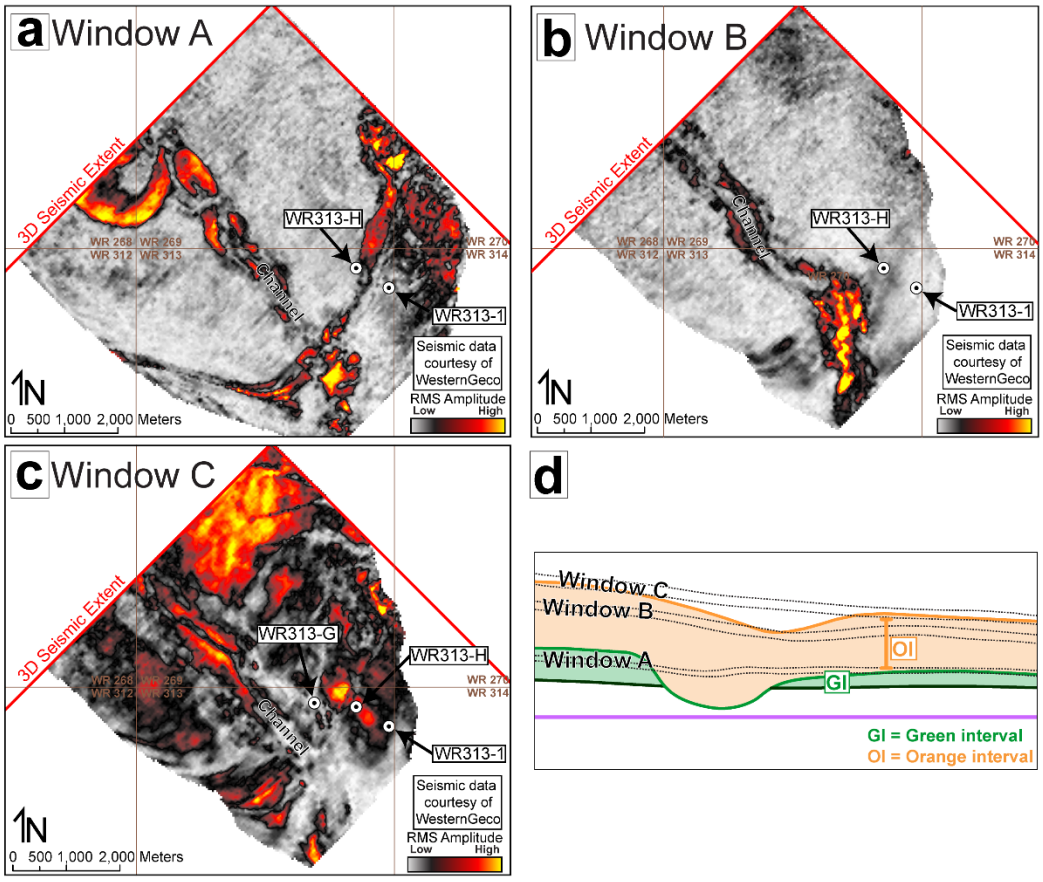

Figure 7. RMS amplitude maps of (a) Window A, (b) Window B, and (c) Window C. (d) Schematic cartoon showing the RMS windows in relation to the Green and Orange intervals. In all three RMS amplitude maps, the channel trends NW-SE. In (a) Window A, high amplitude, discontinuous 'kidney bean' shaped features are within the main channel belt and appear to flank either side of the respective, low amplitude thalweg. The larger loop like feature is truncated by the low amplitude thalweg. In (b) Window B and (c) Window C, the channel appears to straighten. Generally, the high amplitude features are restricted within the channel belt (Window A) or flank either side of the thalweg (Windows B and C).

Within the 3D depth-migrated seismic data, we compared upstream and downstream seismic sections of the Green and Orange intervals (Figure 8). On the upstream end of the channel (Figure 8a), starting at the Green interval, the Base Green horizon is continuous above the Purple horizon (Figure 8b). Above the Base Green horizon, several 'u-shaped' seismic reflections are flanked by 'wing-like,' wavy seismic reflections (Figure 8a, marked in black in Figure 8b). The Top Green horizon sits above these reflections and maintains a similar architecture – u-shaped reflection in the center flanked by wing-like, wavy seismic reflections (Figure 8b). This geometry is maintained even within the Orange interval (bounded by the Top Green and Orange horizons, Figure 3c) with the Orange horizon having the same architectural behavior (u-shaped reflection flanked by wing-like reflections) (Figure 8b). Above the Orange horizon, more u-shaped structures stack on top of each other until they are blanketed by a continuous seismic event (Figure 8a).

On the downstream end of the channel, the Base Green and Top Green horizons are discontinuous above the Purple horizon (Figure 8c). Both horizons seem to be truncated by a boundary marked as the dashed line in Figure 8d. Wavy seismic reflections flank either side of this boundary between the Top Green and Base Green horizons (Figure 8d). Inside the dashed boundary some u-shaped structures stack on top of each other. Once outside of the dashed boundary, the architecture of u-shaped reflections flanked by wing-like reflections similar to that of the upstream seismic section (Figure 8a) stack on top of each other until the Orange horizon (Figure 8d). Above the Orange horizon, several more u-shaped features stack on top of each other until they are blanketed by a continuous seismic event.

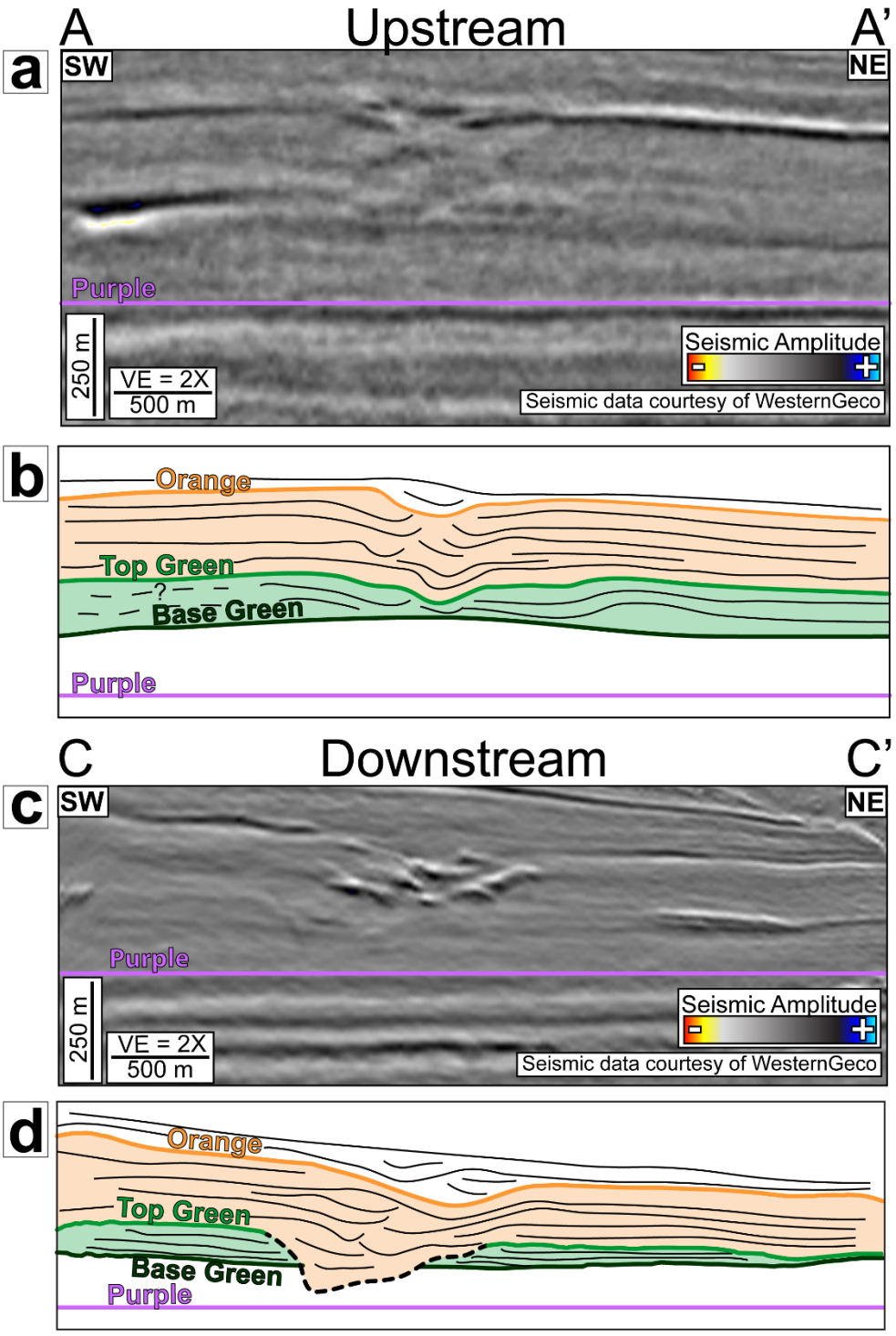
A
Upstream
A'
a
SW
NE
Purple
250 m
VE = 2X
500 m
Seismic Amplitude
Seismic data courtesy of WesternGeco
b
Orange
Top Green
?
Base Green
Purple
C
Downstream
C'
c
SW
NE
Purple
250 m
VE = 2X
500 m
Seismic Amplitude
Seismic data courtesy of WesternGeco
d
Orange
Top Green
Base Green
Purple

Figure 8. (previous page) a) and b): Seismic and line drawing interpretation for upstream (A-A') and downstream locations (C-C') locations. Sections are located on Figure 4. (b and c) The Green interval is highlighted in light green and the Orange interval is highlighted in orange. Upstream (a and b), several 'u-shaped' seismic reflections link to 'wing-like' linear features that stack on top of each other through the Orange interval. Downstream (c and d), the Top Green and Base Green horizons are truncated by an erosional boundary (dashed line) which is then filled in with u-shaped seismic reflections. These reflections stack on top of each other and link with wing-like reflections outside of the boundary. At the top of the Orange interval, the Orange horizon is a regional prominent reflector but is locally absent within the channel.

2.4.2 Log Characterization of the Green and Orange Intervals

The WR 313-H well (Figure 9), encounters the Top Green horizon just beneath the free gas zone (Figure 4) and the Orange horizon above the BHSZ (Figure 5). At this location, the Top Green horizon correlates to the top of a low gamma ray interval that we interpret as the Green sand (Figure 9) in conjunction with the interpretations of Boswell et al. (2012) and Frye et al. (2012). The Base Green horizon correlates to the base of this sand (Figure 9). There is an upward decrease in gamma ray (Figure 9) in the Green sand that is likely an upward increase in sand content. The Orange horizon correlates to the top of a low gamma ray interval that we interpret as the Orange sand (Figure 9) in conjunction with the interpretations of Boswell et al. (2012) and Frye et al. (2012).

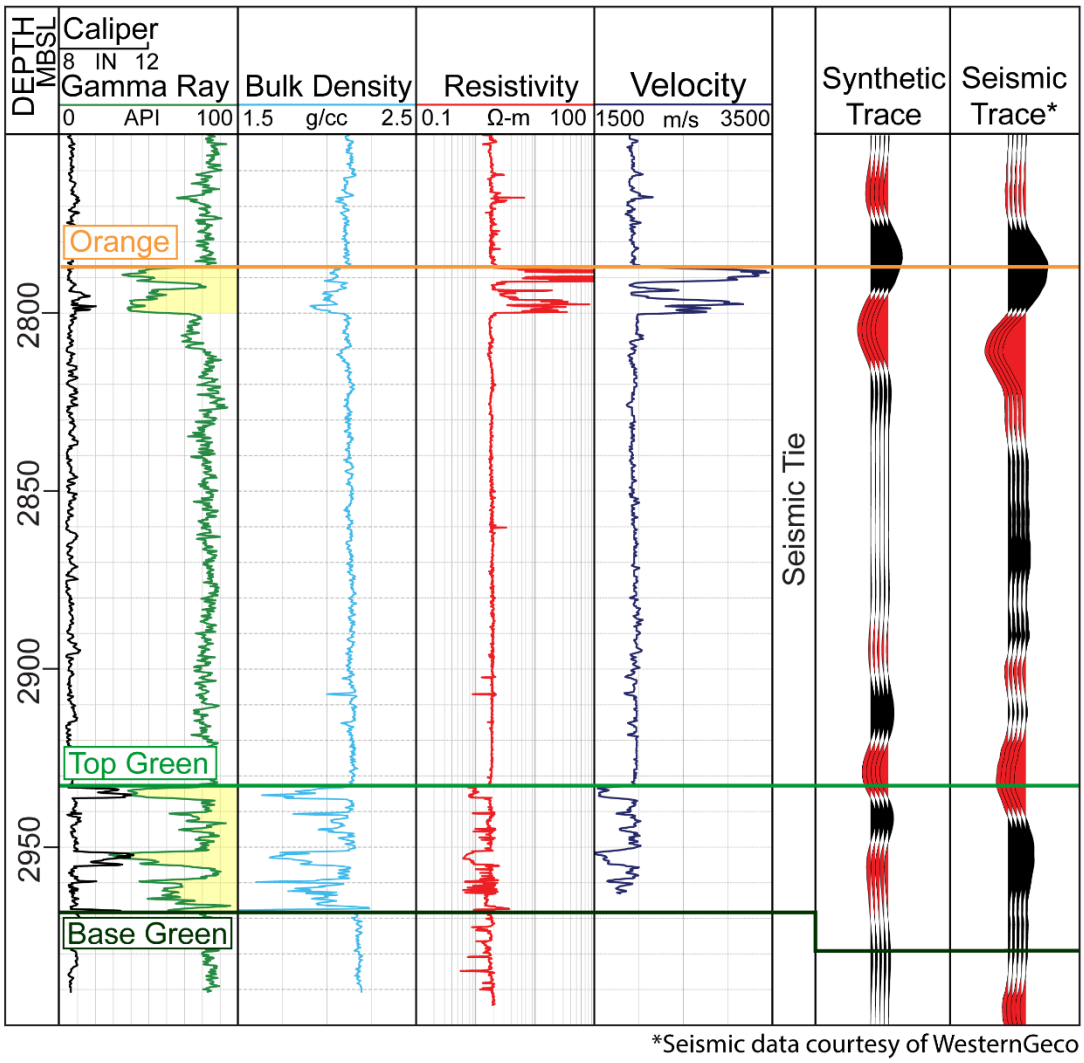

Figure 9. Well logs for WR 313-H of the Green and Orange sands (highlighted in yellow). The top of the Green sand corresponds to a negative polarity reflection (mapped as the Top Green horizon) and the base of the Green sand corresponds to a positive polarity reflection (mapped as the Base Green horizon). The top of the Orange sand corresponds to a positive polarity reflection (mapped as the Orange horizon) at this location (Figure 5) since it is above the BHSZ. Due to the response in velocity and density at the Orange sand, we interpret that the Orange sand contains gas hydrate.

The WR 313-1, -H, and -G wells penetrated the Green and Orange intervals on the northeast flank of the channel axis (Figure 5); we do not know whether the WR 225-1 well is within or outside of the channel (Figures 5 and 10). The Orange sand is missing at the WR 313-G location (Figure 10); this penetration is closest to the channel axis (Figure 5). The seismic reflection that correlates to the top of both of these sands is continuous between the WR 313-1, -H, -G locations, which suggests these sands are continuous between these locations (Figure 10). However, there is a systematic change in the character of both the Green sand and the Orange sand from thick and blocky at the WR 225-1 location to interbedded, thinner sands toward WR 313-1 (Figure 10). The Green sand in particular expands from a few meters of interbedded sand and mud at the WR 313-1 well to 74 meters of clean blocky sand at the WR 225-1 well (Figure 10). The logs measure thick marine mud sections both beneath the Green sand and between the Green and Orange sands; approximately 70% of the net thickness from the Purple equivalent to the Green sand is composed of marine mud.

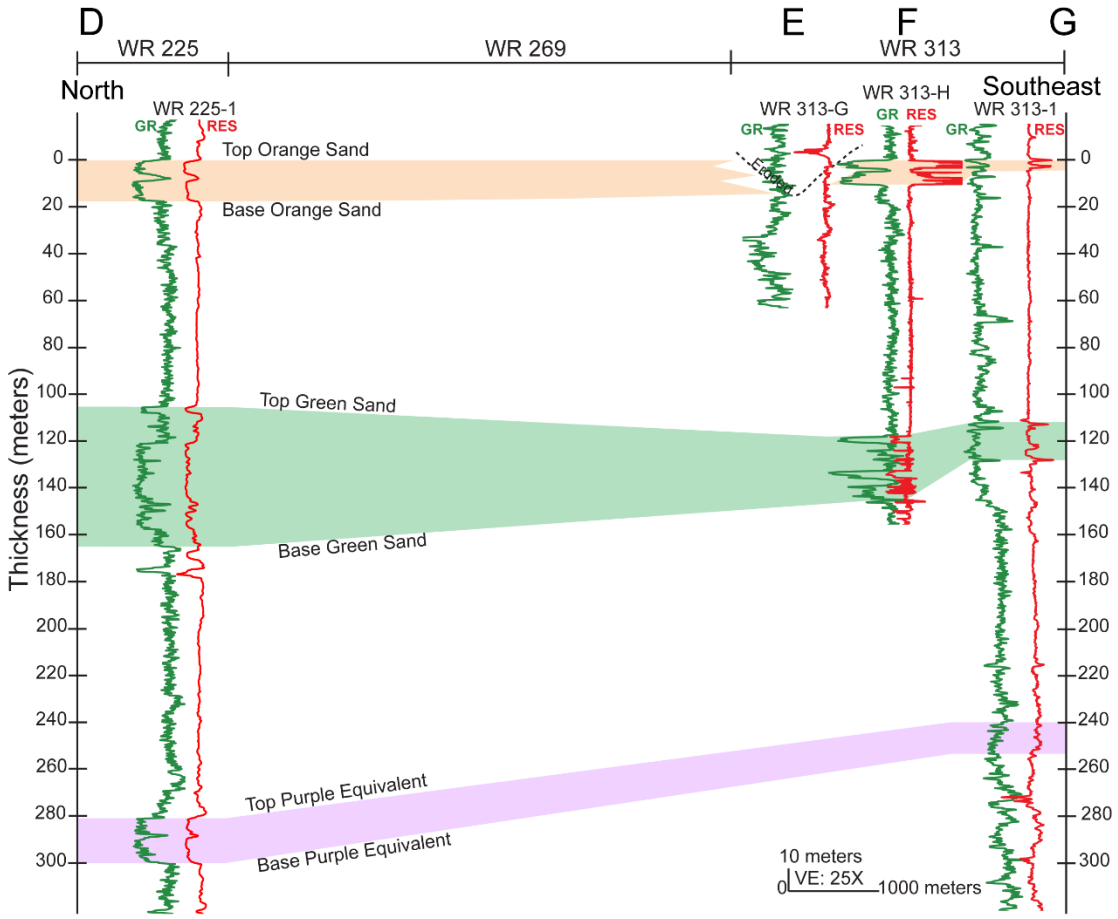

Figure 10. Stratigraphic cross section (located on Figure 5) of the Orange sand, Green sand, and Purple equivalent (hung on the top of the Orange sand). Within the main study area, this cross section captures the sands to the NE of the central channel axis (Figure 5). The Green and Orange sands thin from the north to the southeast. We interpret that the Orange sand is eroded within the WR 313-G well. Both the Green and Orange sands are significantly thicker in the northern portion of the basin and we interpret that they are unrelated to channelized deposition.

2.5 DISCUSSION

2.5.1 Interpretation of the Green and Orange Intervals

Initially, during Green sand deposition (the Green interval), large turbidity flows resulted in the deposition of sheet sands across the basin at both the upstream and downstream locations (Figures 11a, 11b, and 12a). Deposition of the Green sand continued in the upstream location. In contrast, at the southeastern margin of the basin, at the minibasin exit point, accommodation was limited by the uplifted salt margin. In this downstream location (Figure 11c), erosion occurred (Figure 12a). Relative uplift of salt at the southeastern basin margin results in the development of an erosional channel at the basin exit point and then the gradual upstream migration of a knickpoint from southeast to northwest: deposition of the Green sand continues to the northwest of this knickpoint while erosion and bypass occurs to the southeast (Figure 12a).

Deposition of the Green sand was followed by a prolonged period of channelized deposition that we characterize as the Orange interval. The erosional bypass surface (dashed line, Figures 11c and 12) was filled at the onset of the Orange interval (Figure 12c). Initially, the channel is confined by the canyon formed at the end of the Green interval (dashed line, Figures 11d and 12b). Channelized deposits (‘kidney bean’ features as described in Figure 7a) fill in the extent of this canyon (Figure 12c).

The large loop like feature in the northwestern portion of Figure 7a and in the map view illustration of Figure 12c is interpreted to record a meander cut off driven by salt tectonism as the channel evolved through time. After the channel is no longer confined by the previous incision, the channel then aggrades to reach and maintain its equilibrium profile (Figures 7b and 12c). During this time, the aggrading channel is bounded by levees at its margins (Figures 4, 5 and 7): coarse-grained deposition was restricted to the channel

axis and the immediately adjacent levees; mud was deposited further from the channel (Figures 11a, 11c and 12c). This is dramatically illustrated by the thick marine mud interval observed in the logs between the Green and Orange sands (Figure 10) on the flank of the channel; these thick mud intervals were deposited contemporaneously with the aggrading vertical channel (Figure 11) observed in the seismic data.

The Orange interval is capped by the Orange sand (Figure 12d). Like the Green sand, this sand is a laterally extensive sheet sand that is thickest in the basin center and thins at the basin margins (Figures 10 and 12d). Areas with lower accommodation are characterized by thinner Orange sand deposition and lower net to gross. Following Orange sand deposition, minor channelization continues with deposition of mud (Figure 11c) marking continued bypass of coarse-grained sediment across the spill point to the southeast until the channel shuts off (Figure 12e).

Taken together, we envision that the Green and Orange intervals record the transition from ponded sand deposition, enabled by significant accommodation from salt withdrawal, to sediment bypass that occurred as accommodation became limited. The Green and Orange sands record two periods of large scale turbidite deposition. These sands are similar to the perched apron sand system described by Prather et al. (2012) and stacked submarine lobes incised by a channel system described by Deptuck et al. (2012). These deposits thicken up dip from the minibasin exit point and are formed coincidentally with an erosional channel. This erosional channel propagates updip with time and records the bypass of sediment through the minibasin. Between deposition of the Green and Orange sands and following deposition of the Orange sand, there was persistent aggradation of a leveed channel system where flows bypassed the basin; if there was any sand deposition, it was restricted within or near the channel axis.

The Green and Orange sands may record high energy events resulting from the release of large, unconfined flow updip relative to the leveed channel system. The large magnitude of the unconfined flows allows the flows to overtop the local leveed channel which in turn allows these flows to spread laterally. In contrast, the prolonged period of channelized deposition may record lower energy times where the flows were constricted or did not have enough momentum to overtop the local leveed channel system. An alternative interpretation is that the Green and Orange sands record times of increased accommodation in the basin whereas the leveed channel deposition records times of limited accommodation and bypass.

Ultimately, we lean towards the interpretation that the Green and Orange sands record the release of large amounts of sand updip of the southwestern lobe of the Terrebonne Basin and were deposited in an unconfined setting. Prather et al. (2012) discusses how autogenic processes (sediment storage and release cycles) in conjunction with allogenic processes (eustatic sea-level rise/fall) contribute to the transport of large packages of coarser sediment far from the continental shelf margin. Furthermore, sediment-gravity flows can pick up this coarser material from previous episodes of ponded deposition that collapse due to slope failure or salt movement (Pirmez and Imran, 2003; Prather et al., 2012; Pratson and Ryan, 1994). Thus, we interpret the Green and Orange sands are a collection of coarser sediment that was stored within updip basins, failed due to salt movement or deformation, were then picked up and transported downdip by sediment gravity flows, and were deposited as large sheet sands due to their lateral extent. We interpret that the Green sand was built by a series of the high energy events that were less confined updip as the submarine channel initiated (Green interval); while the Orange sand was a single, unconfined high energy event that blanketed the aggrading channel (Orange interval) and was incised and reworked by the channel before it shut off.

Our interpretation of the Green and Orange sands as sheet sand deposits is most similar to that of Frye et al. (2012) who interpreted that these deposits record sheet (or stacked lobe) sand deposition and it contrasts that of Boswell et al. (2012) who suggested these reservoirs represent levee deposits. In our interpretation both of these sands were initially deposited with a sheet-like geometry and a bypass channel subsequently eroded into these sands resulting in the observation of the sands having a channel axis which is recorded in seismic data (e.g. Figures 4 and 5). This evolutionary model explains the enigmatic observation that the sand thickness increases away from the channel axis as recorded by both log and inferred from seismic amplitude (Figures 4 and 5).

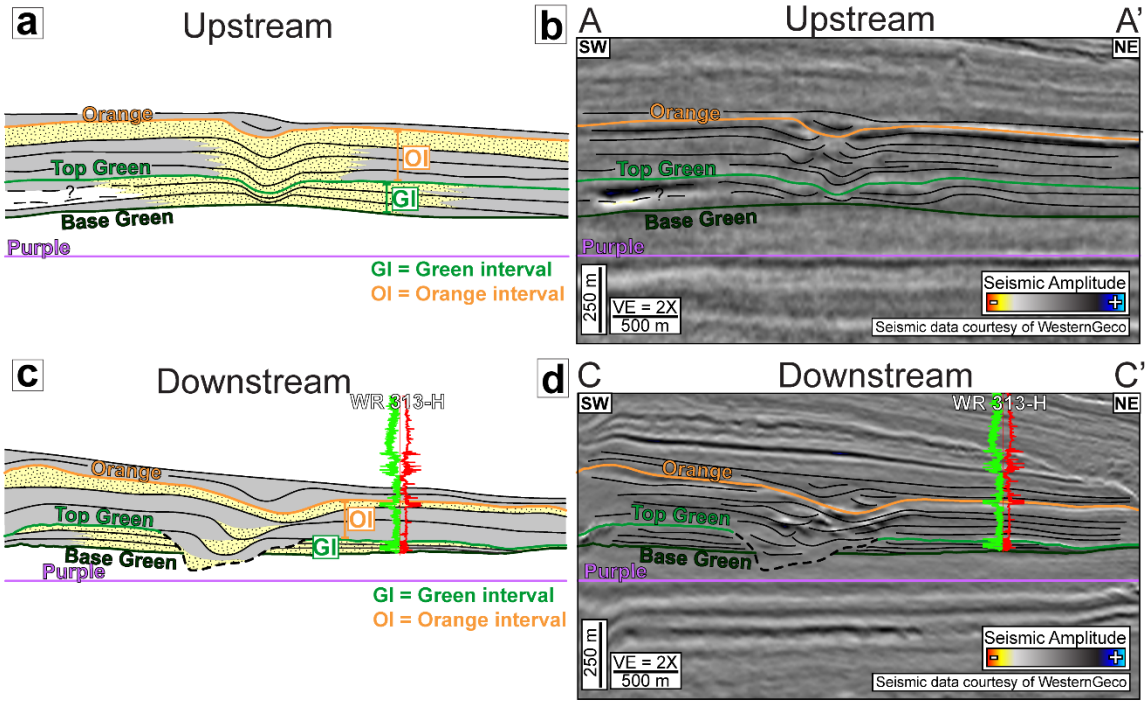

Figure 11. Simplified line drawing evolution of the Green and Orange intervals on the (a) upstream and (c) downstream ends of the channel. Line drawings are based off of (b) upstream and (d) downstream seismic sections (location on Figure 4). The WR 313-H (gamma ray (green) and resistivity (red) log curves displayed) well penetrated the Top Green and Orange and horizons to the NE flank of the channel. On the (b) upstream end, several u-shaped seismic reflections are flanked by wing-like reflections that stack on top of each other from the Base Green to the Orange horizons. On the (d) downstream end, the Top Green and Base Green horizons are truncated by a boundary marked by the dashed line that signifies the end of the Green interval. The dashed line is then filled in by several u-shaped reflections that stack on top of each other. The u-shaped reflections are then flanked by wing-like reflections outside of the boundary until they encounter Orange horizon. This geometry is maintained in the upstream and downstream sections until the channel shuts off and is blanketed by a continuous seismic event.

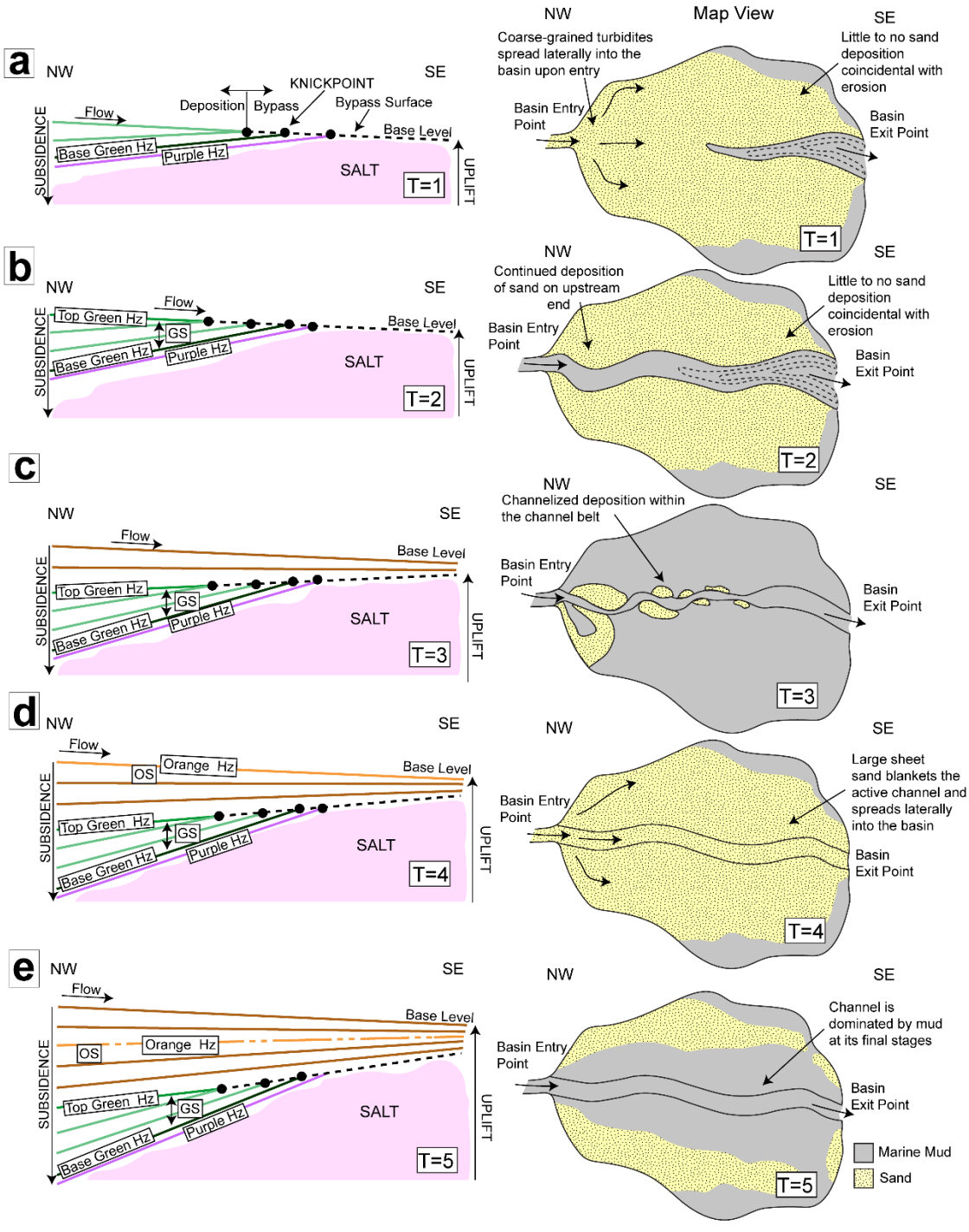
a
NW
SE
KNICKPOINT
Deposition
Bypass
Bypass Surface
Flow
Base Level
Base Green Hz
Purple Hz
SALT
SUBSIDENCE
UPLIFT
T=1
Map View
Coarse-grained turbidites spread laterally into the basin upon entry
Little to no sand deposition coincidental with erosion
Basin Entry Point
Basin Exit Point
b
Top Green Hz
GS
T=2
Continued deposition of sand on upstream end
c
Channelized deposition within the channel belt
T=3
d
OS
Orange Hz
T=4
Large sheet sand blankets the active channel and spreads laterally into the basin
e
T=5
Channel is dominated by mud at its final stages
Marine Mud
Sand

Figure 12. (previous page) Interpreted 2D line (left) and corresponding map view (right) of the evolution of the submarine channel system in the southwestern lobe of the Terrebonne Basin. (a) (T=1) Turbulent flows enter the southwestern lobe of Terrebonne depositing sheet-like sands coincidentally with active salt movement. We interpret a knickpoint initiates, propagates to the upstream end, and a bypass surface develops. b) (T=2) The Top Green Hz marks the end of the Green interval. The Green sand (GS) consists of the coarser material stripped from the turbulent flows that were deposited during the Green interval. c) (T=3) After the Green interval, the channel transitions from a bypass phase to a depositional phase (the beginning of the Orange interval). d) (T=4) During the Orange interval, the channel aggrades on both the upstream and downstream ends until the deposition of the Orange sand (OS) (top of Orange sand correlates to the Orange Hz). e) (T=5) After the deposition of the Orange interval, the channel incises the Orange Hz and continues to aggrade until it shuts off.

2.5.2 Implications for the Hydrate Reservoir

The Green and Orange sands were targeted as hydrate reservoirs and the WR 313-H and WR 313-1 wells confirmed the presence of hydrates in these reservoirs. The sheet like geometry of the Green and Orange sands that thicken and coarsen across the Terrebonne Basin provides a connected regional aquifer to capture and focus hydrocarbons toward the crest of the structure (Figure 10).

In addition, if the Green and Orange sands are sheet sand deposits, we interpret that they record high energy flows. This would contrast the levee sand deposits recently cored at Green Canyon Block 955 (Flemings et al., 2020; Meazell et al., 2020; Santra et al., 2020). These deposits were found to be sandy silt and thinly bedded. Meazell et al. (2020) interprets that this gas hydrate reservoir was formed by levee-channel deposition. In this case, a majority of the coarse grained material in the turbidity flows were confined within the channel axis and the finer material built the corresponding levees (Meazell et al., 2020). Because we interpret that the Green and Orange sands are high energy, unconfined, turbidite deposits, we envision that they will be coarser grained than those penetrated at

GC 955 and perhaps more analogous to the medium-grained sands encountered in the Brazos Trinity Basin IV (Flemings et al., 2006). Thus, the WR 313 reservoir may be a more favorable reservoir for hydrate production because its coarser sediment will have a higher intrinsic permeability.

2.6 CONCLUSIONS

Subsurface interpretation of the interaction between active sedimentary and salt tectonic processes is important in mapping and characterizing reservoirs. To understand the Green and Orange hydrate reservoirs in the southwestern lobe of the Terrebonne Basin, we interpret that the Green and Orange sands are sheet sands and most likely thicken towards the north. These sands were incised by an aggrading leveed-channel with sediment bypassing the system at that time. The channel contains little to no sand within the central axis and immediately adjacent levees, but is dominated by muds and silts that build much of the distal levees.

The amount of accommodation varied through time and position within the basin and strongly impacted the depositional system and thus the ultimate stratigraphy. The Green and Orange sands as well as the mud rich levee deposits of the submarine channel system thicken towards the north due to a significant increase in accommodation in this area. In the Terrebonne Basin, active salt movement increases or decreases accommodation and thus directly influences the thickness of sedimentary packages as well as the behavior (incision, bypass, aggradation) of the channel.

Reservoir extent, thickness, and quality are influenced by depositional processes which are in turn driven by accommodation. The Green and Orange sands contain hydrate at the crest of the structure within the southwestern lobe of the Terrebonne Basin. These sands are most likely regional sheet sands that thicken towards to the north into the broader

Terrebonne Basin due to an increase in accommodation. This suggests that thicker packages of sand are captured updip and have the potential to act as reservoirs at the structural highs within the broader Terrebonne Basin.

2.7 ACKNOWLEDGEMENTS

We would like to thank David Mohrig, Jake Covault, and Ann Cook for their helpful discussions and reviews to improve this manuscript. We would also thank WesternGeco for access to the 3D seismic data.

2.8 FUNDING

This work is supported by the Department of Energy Genesis of Methane Hydrate Project Award Number DE-FE0023919. This report was prepared as an account of work sponsored by an agency of the United States Government. Neither the United States Government nor any agency thereof, nor any of their employees, makes any warranty, express or implied, or assumes any legal liability or responsibility for the accuracy, completeness, or usefulness of any information, apparatus, product, or process disclosed, or rep-resents that its use would not infringe on privately owned rights. Reference herein to any specific commercial product, process, or service by trade name, trademark, manufacturer, or otherwise does not necessarily constitute or imply its endorsement, recommendation, or favoring by the United States Government or any agency thereof. The views and opinions of authors expressed herein to not necessarily state or reflect those of the United States Government or any agency thereof.

Chapter 3: Appendix

APPENDIX A: INSTANTANEOUS AMPLITUDE MAPS OF THE PURPLE AND BASE GREEN HORIZONS

This appendix contains instantaneous amplitude maps of the Purple and Base Green horizons. Figure A1 is the instantaneous amplitude map of the Purple horizon. There are two main distinguishing characteristics in this map: first, there are linear, dim zones (faults) towards the N-NE portion of the map. Second, there is no obvious contrast in amplitude within the 3D depth seismic extent. Therefore, I interpret that the Purple horizon represents a uniform, lateral deposition of sediment filling the available accommodation (ponded deposition). Figure A2 shows the instantaneous amplitude map of the Base Green horizon. There are three main distinguishing characteristics in this map: first, there is a contrast in amplitude where I would expect the BHSZ. The Base Green horizon is mapped on a peak amplitude (positive polarity reflection) therefore the amplitude character varies where it interacts with the BHSZ. Second, the channel starts to appear and trends NW-SE within WR 313. Third, within the channel belt, there are discontinuous pockets of low amplitude that trend with the channel. The Base Green horizon correlates to the base of the Green sand (Figure 9). At the time of the Base Green horizon, incision began to occur at the downstream end and coarse-grained deposition (pockets of low amplitude in Figure A2) was either restricted to the central axis of the channel or along its edges (Figure 12A).

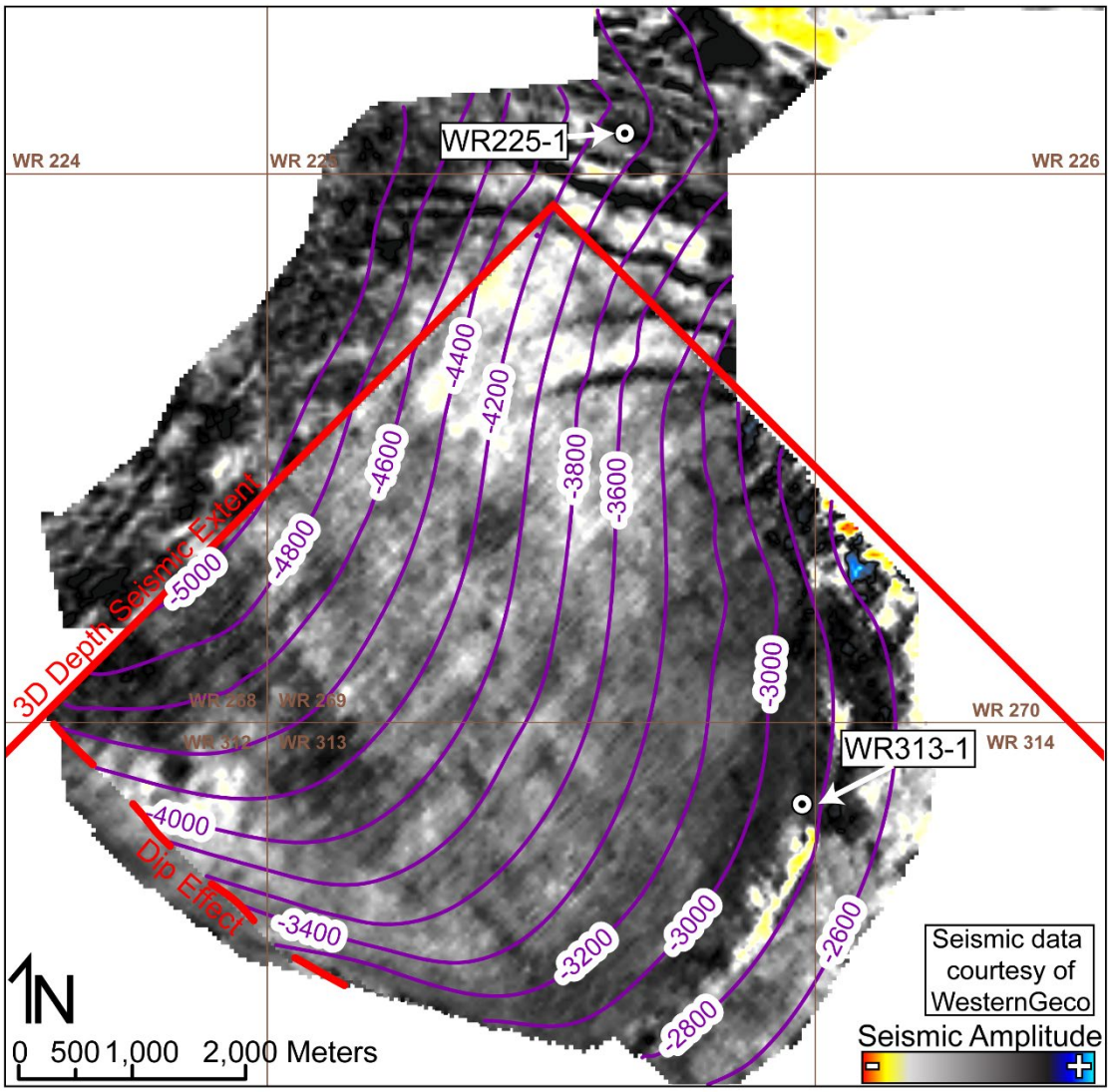

Figure A1. Instantaneous amplitude at the Purple horizon. Contours are in meters below sea level (mbsl) (CI = 200 meters). The amplitude extraction north of the red outline (3D Depth Seismic Extent) was taken on the 3D time dataset. The red outline shows the extent of the 3D depth survey, brown lines show lease block boundaries, white circles show surface location of wells.

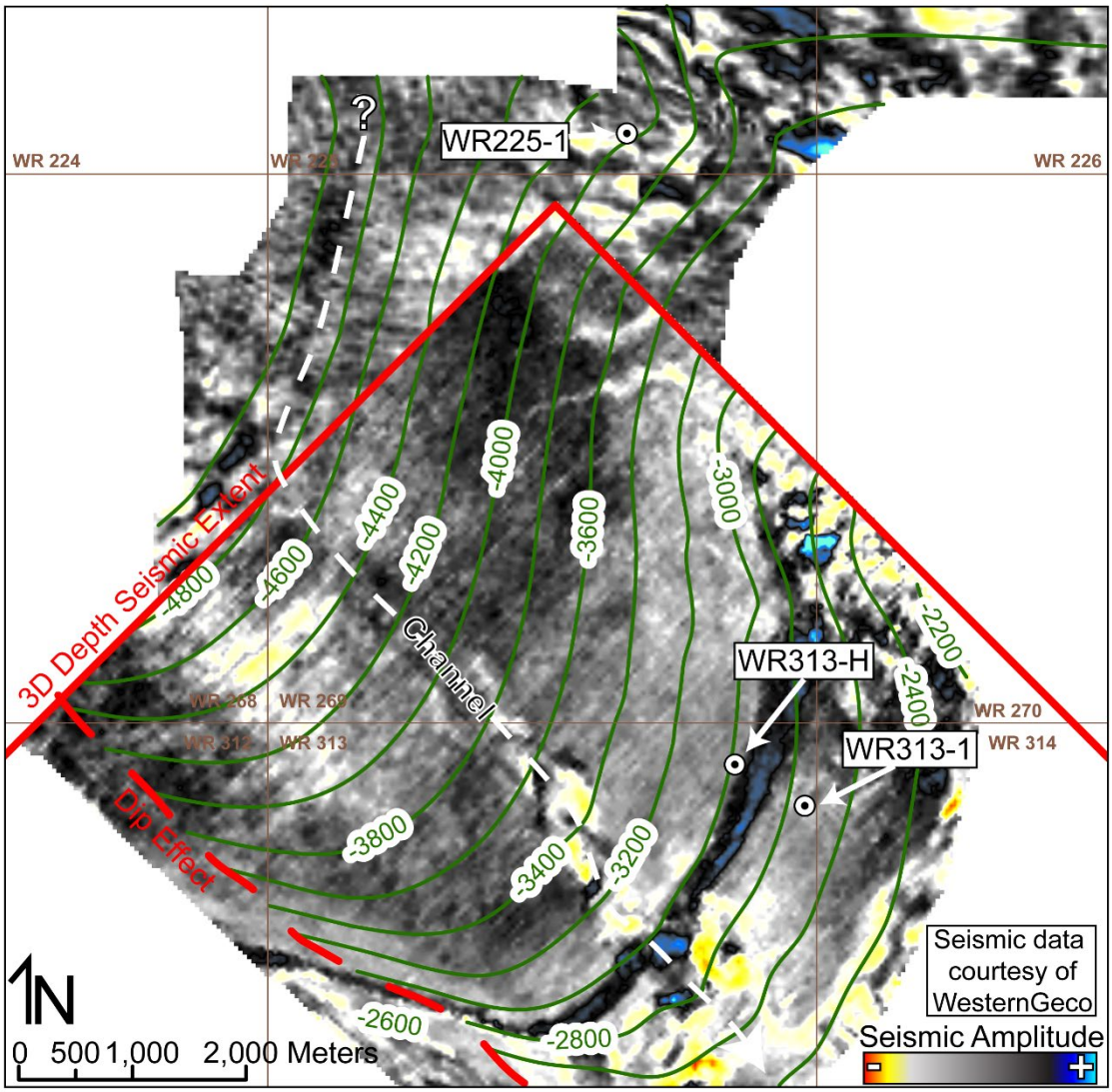

Figure A2. Instantaneous amplitude at the Base Green Horizon. Contours are in meters below sea level (mbsl) (CI = 200 meters). The amplitude extraction north of the red outline (3D Depth Seismic Extent) was taken on the 3D time dataset. The red outline shows the extent of 3D depth survey, brown lines show lease block boundaries, white circles show surface location of wells.

APPENDIX B: DIFFERENCE MAPS

This appendix contains the difference (thickness) maps used to support the interpretations discussed in Chapter 2. Figure B1 shows the thickness map of the Purple to Base Green horizons and the corresponding upstream and downstream cross sections that were displayed in Figure 6b and 6c. Figures B2 and B3 are regional thickness maps of the Purple to Top Green horizons (B2) and the Top Green to Orange horizons (B3). Figure B2 extends from the localized study area of Figure 6a. Within Figures B2 and B3, there is a large fault that separates the southwestern lobe from the broader Terrebonne Basin represented by the sudden decrease in thickness towards the northwest. However, both Figures B2 and B3 show a drastic increase in thickness updip of this fault towards to the broader Terrebonne Basin. This is most likely due to an increase in accommodation towards the north and larger amounts of sediment are captured updip and are separated by the fault from the localized study area.

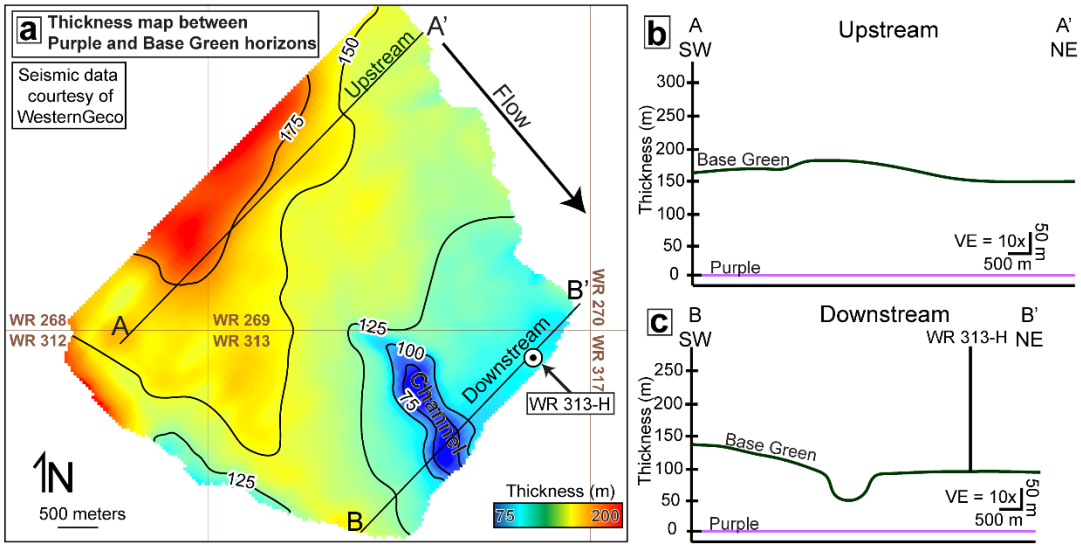

Figure B1. (a) Thickness map of the Purple to Base Green horizons (CI = 25 m). Brown lines show lease block boundaries and white circle shows surface location of WR 313-H. (b) On the upstream end, the Base Green is continuous from SW to NE; there is no obvious channelized incision. (c) On the downstream end, the channel incises the Base Green horizon and the underlying strata.

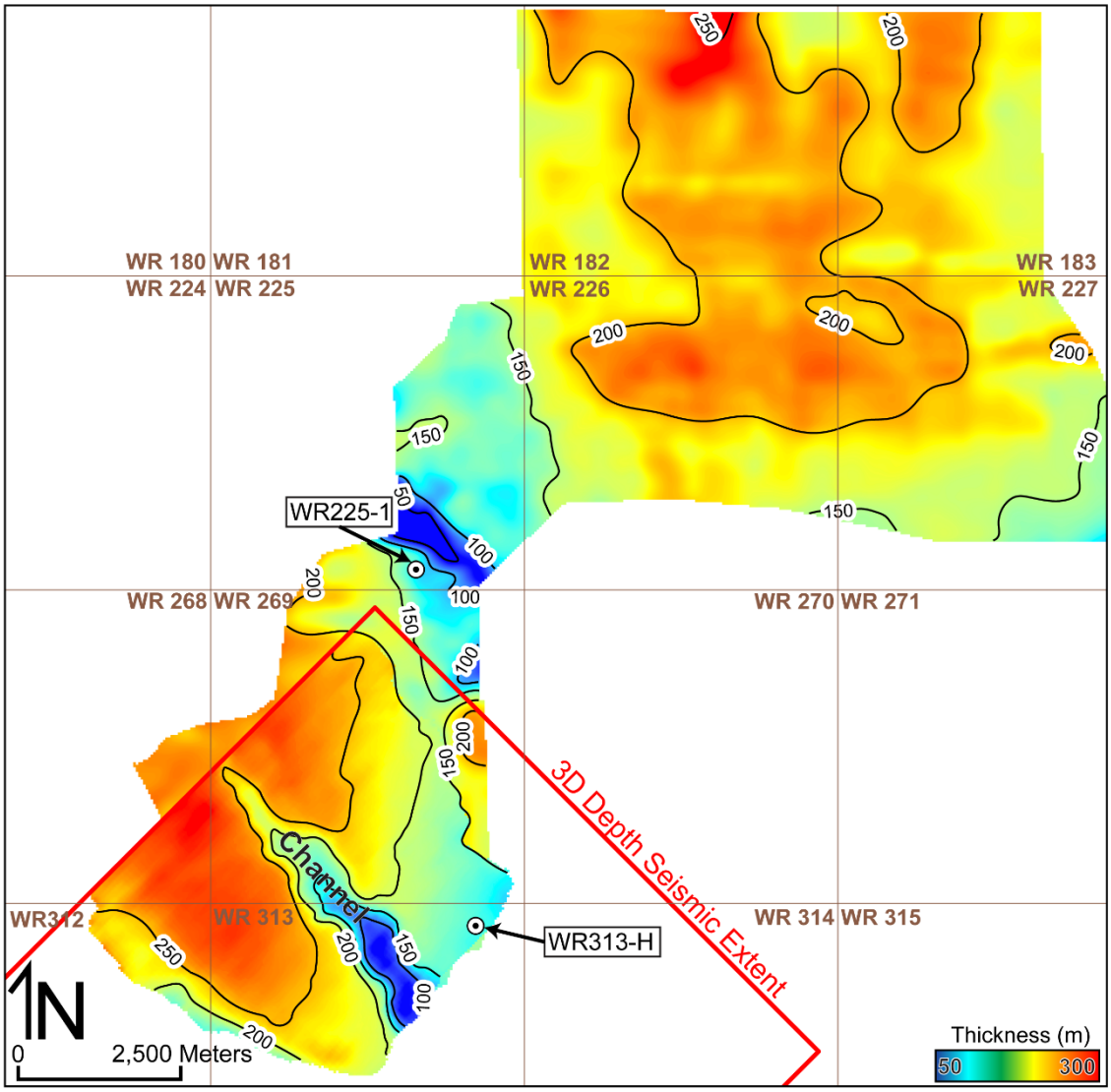

Figure B2. Regional thickness map of the Purple to Top Green horizons (CI = 50 m). Brown lines show lease block boundaries and white circle shows surface locations of wells. Red outline shows the 3D depth seismic data extent.

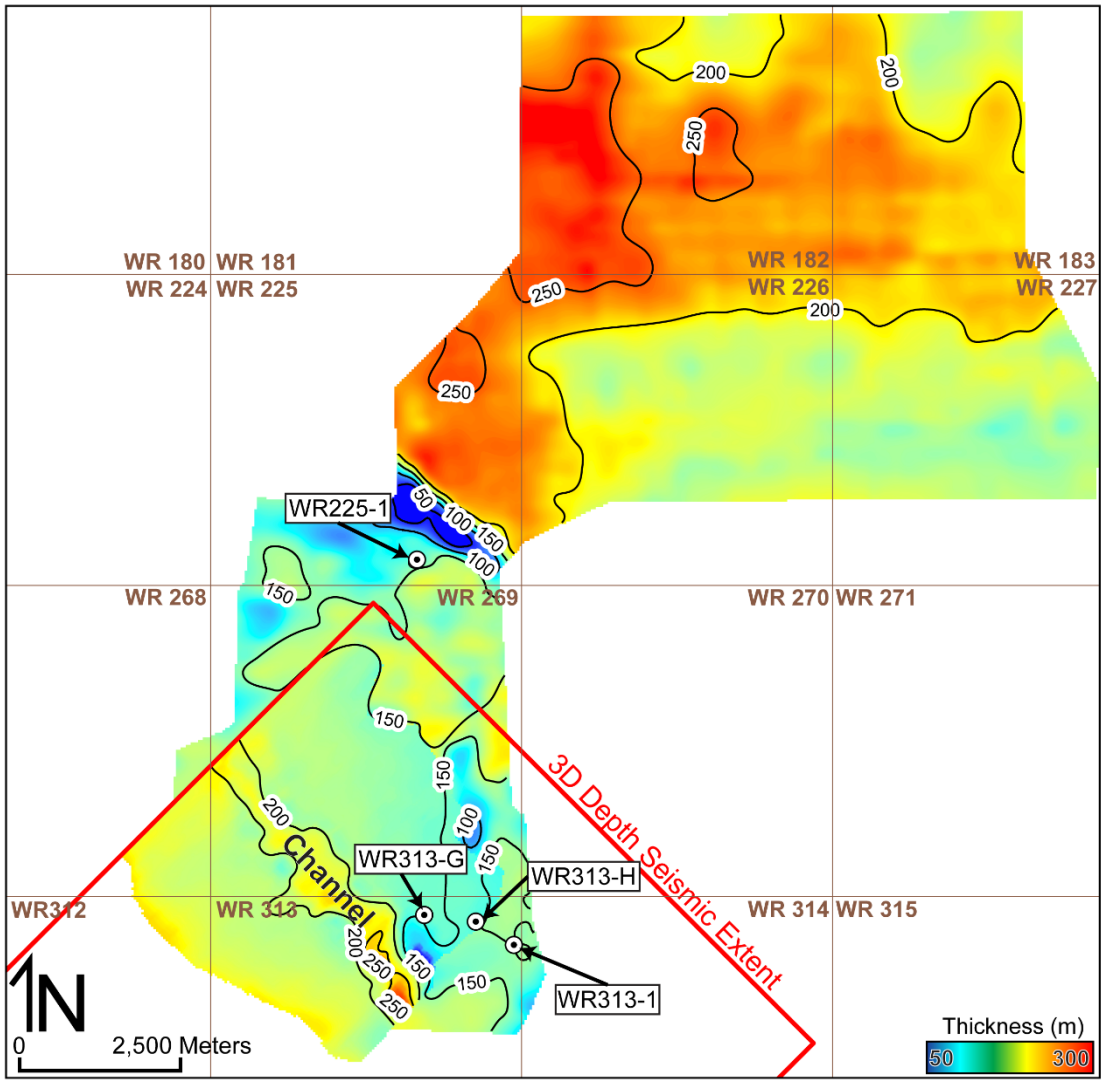

Figure B3. Regional thickness map of the Top Green to Orange horizons (CI = 50 m). Brown lines show lease block boundaries and white circle shows surface locations of wells. Red outline shows the 3D depth seismic data extent.

References

Booth, J. R., M. C. Dean, I. I. I. A. E. DuVernay, and M. J. Styzen, 2003, Paleo-bathymetric controls on the stratigraphic architecture and reservoir development of confined fans in the Auger Basin: central Gulf of Mexico slope: Marine and Petroleum Geology, v. 20, p. 563-586.

Boswell, R., M. Frye, D. Shelander, W. Shedd, D. R. McConnell, and A. Cook, 2012, Architecture of gas-hydrate-bearing sands from Walker Ridge 313, Green Canyon 955, and Alaminos Canyon 21: Northern deepwater Gulf of Mexico: Marine and Petroleum Geology, v. 34, p. 134-149.

Brooks, J. M., M. C. Kennicutt, R. R. Fay, T. J. McDonald, and R. Sassen, 1984, Thermogenic Gas Hydrates in the Gulf of Mexico: Science, v. 225, p. 409-411.

Deptuck, M. E., Z. Sylvester, and C. O'byrne, 2012, Pleistocene Seascape Evolution Above A "Simple" Stepped Slope—Western Niger Delta, *in* B. E. Prather, M. E. Deptuck, D. Mohrig, B. V. Hoorn, and R. B. Wynn, eds., Application of the Principles of Seismic Geomorphology to Continental Slope and Base-of-Slope Systems: Case Studies from SeaFloor and Near-Sea Floor Analogues, v. 99, SEPM Society for Sedimentary Geology, p. 0.

Diegel, F. A., J. F. Karlo, D. C. Schuster, R. C. Shoup, and P. R. Tauvers, 1995, Cenozoic structural evolution and tectono-stratigraphic framework of the northern Gulf coast continental margin, *in* M. P. A. Jackson, D. G. Roberts, and S. Snelson, eds., Salt tectonics: a global perspective: AAPG Memoir 65, p. 109-151.

Flemings, P. B., J. H. Behrmann, C. M. John, and E. Scientists, 2006, Expedition 308 summary: College Station, Texas: Integrated Ocean Drilling Program Management International, Inc., v. 08, p. 1-70.

Flemings, P. B., S. C. Phillips, R. Boswell, T. S. Collett, A. E. Cook, T. Dong, M. Frye, G. Guerin, D. S. Goldberg, M. Holland, J. Jang, K. Meazell, J. Morrison, J. O'Connell, T. Pettigrew, E. Petrou, P. J. Polito, A. Portnov, M. Santra, P. J. Schultheiss, Y. Seol, W. Shedd, E. A. Solomon, C. M. Thomas, W. F. Waite, and K. You, 2020, Pressure coring a Gulf of Mexico deep-water turbidite gas hydrate reservoir: Initial results from The University of Texas–Gulf of Mexico 2-1 (UT-GOM2-1) Hydrate Pressure Coring Expedition: AAPG Bulletin, v. 104, p. 1847-1876.

Flint, S. S., D. M. Hodgson, A. R. Sprague, R. L. Brunt, W. C. V. d. Merwe, J. Figueiredo, A. Prélat, D. Box, C. D. Celma, and J. P. Kavanagh, 2011, Depositional architecture and sequence stratigraphy of the Karoo basin floor to shelf edge succession, Laingsburg depocentre, South Africa: Marine and Petroleum Geology, v. 28, p. 658-674.

Frye, M., W. Shedd, and R. Boswell, 2012, Gas hydrate resource potential in the Terrebonne Basin, Northern Gulf of Mexico: Marine and Petroleum Geology, v. 34, p. 150-168.

Hillman, J. I. T., A. E. Cook, D. E. Sawyer, H. M. Küçük, and D. S. Goldberg, 2017, The character and amplitude of 'discontinuous' bottom-simulating reflections in marine seismic data: Earth and Planetary Science Letters, v. 459, p. 157-169.

Hutchinson, D., R. Boswell, T. Collett, J. C. Dai, B. Dugan, M. Frye, E. Jones, D. McConnell, K. Rose, C. Ruppel, W. Shedd, D. Shelander, and W. Wood, 2009, Gulf of Mexico Gas Hydrate Joint Industry Project Leg II — Walker Ridge 313 site selection., Proceedings of the Drilling and Scientific Results of the 2009 Gulf of Mexico Gas Hydrate Joint Industry Project Leg II.

Jobe, Z. R., Z. Sylvester, N. Howes, C. Pirmez, A. Parker, A. Cantelli, R. Smith, M. A. Wolinsky, C. O'Byrne, N. Slowey, and B. Prather, 2017, High-resolution, millennial-scale patterns of bed compensation on a sand-rich intraslope submarine fan, western Niger Delta slope: GSA Bulletin, v. 129, p. 23-37.

McConnell, D., and Z. Zhang, 2005, Using acoustic inversion to image buried gas hydrate distribution: Fire in the Ice, v. 2005, p. 3-5.

McConnell, D. R., and B. A. Kendall, 2002, Images of the Base of Gas Hydrate Stability, Northwest Walker Ridge, Gulf of Mexico, Offshore Technology Conference, Houston, Texas.

Meazell, K., P. B. Flemings, M. Santra, and J. E. Johnson, 2020, Sedimentology and stratigraphy of a deep-water gas hydrate reservoir in the northern Gulf of Mexico: AAPG Bulletin, v. 104, p. 1945-1969.

Meazell, P. K., and P. B. Flemings, 2022, The evolution of seafloor venting from hydrate-sealed gas reservoirs: Earth and Planetary Science Letters, v. 579, p. 13.

Milkov, A. V., and R. Sassen, 2001, Estimate of gas hydrate resource, northwestern Gulf of Mexico continental slope: Marine Geology, v. 179, p. 71-83.

Pirmez, C., and J. Imran, 2003, Reconstruction of turbidity currents in Amazon Channel: Marine and Petroleum Geology, v. 20, p. 823-849.

Prather, B. E., C. Pirmez, and C. D. Winker, 2012, Stratigraphy of Linked Intraslope Basins: Brazos–Trinity System Western Gulf of Mexico, Application of the Principles of Seismic Geomorphology to Continental-Slope and Base-of-Slope Systems: Case Studies from Seafloor and Near-Seafloor Analogues, v. 99, SEPM (Society for Sedimentary Geology), p. 83-109.

Pratson, L. F., and W. B. F. Ryan, 1994, Pliocene to recent infilling and subsidence of intraslope basins offshore Louisiana: AAPG Bulletin, v. 78, p. Medium: X; Size: pp. 1483-1506.

Santra, M., P. B. Flemings, K. Meazell, and E. Scott, 2020, Evolution of gas hydrate–bearing deep-water channel-levee system in abyssal Gulf of Mexico: Levee growth and deformation: AAPG Bulletin, v. 104, p. 1921-1944.

Shedd, W., R. Boswell, M. Frye, P. Godfriaux, and K. Kramer, 2012, Occurrence and nature of “bottom simulating reflectors” in the northern Gulf of Mexico: Marine and Petroleum Geology, v. 34, p. 31-40.

Worrall, D. M., and S. Snelson, 1989, Evolution of the northern Gulf of Mexico, with emphasis on Cenozoic growth faulting and the role of salt, *in* A. W. Bally, and A. R. Palmer, eds., The geology of North America: an overview: GSA Decade of North American Geology, v. A, p. 97-138.